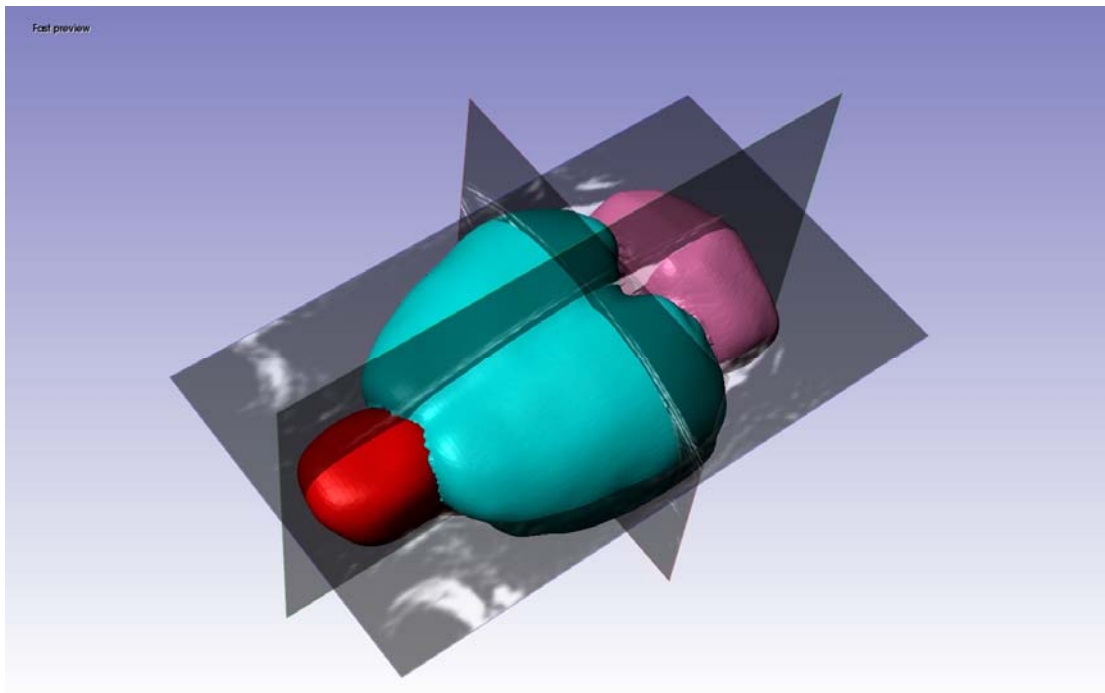


# CHALMERS



## Development of an Animal Brain FE model

Master's Thesis in the Applied Mechanics

**GIANFRANCO RAMIREZ**

Department of Applied Mechanics

*Division of Vehicle Safety*

CHALMERS UNIVERSITY OF TECHNOLOGY

Göteborg, Sweden 2010

Master's Thesis 2010:66



MASTER'S THESIS 2010:66

# Development of an animal brain FE model

Master's Thesis in the Applied Mechanics

GIANFRANCO RAMIREZ

Department of Applied Mechanics  
*Division of Vehicle Safety*

CHALMERS UNIVERSITY OF TECHNOLOGY

Göteborg, Sweden 2010

Development of an animal brain FE model  
Master's Thesis in the Applied Mechanics  
GIANFRANCO RAMIREZ

© GIANFRANCO RAMIREZ 2010

Master's Thesis 2010:66  
ISSN 1652-8557  
Department of Applied Mechanics  
Division of Vehicle Safety  
Chalmers University of Technology  
SE-412 96 Göteborg  
Sweden  
Telephone: + 46 (0)31-772 1000

Department of Applied Mechanics  
Göteborg, Sweden 2010

Development of an animal brain FE model  
Master's Thesis in the Applied Mechanics  
GIANFRANCO RAMIREZ

Department of Applied Mechanics  
Division of Vehicle Safety  
Chalmers University of Technology

## ABSTRACT

During this thesis a rat finite element (FE) model was developed and the relative methodology to operate was presented. The new rat brain FE model was developed using image processing techniques by extracting the geometry and mesh from magnetic resonance imaging (MRI). A new rat brain model was needed due to several limitations present in previous models *Baumgartner D. et al (2009)*. Finite element simulations using a more detailed model were required to improve the understanding of the mechanisms responsible for injuries in the brain. The rat brain model developed in this thesis will be used in the future to simulate animal experiments carried out by *Davidsson J. et al (2009)*. A method to get the geometry and the final model was developed in order to have the highest possible level of repeatability. Several limitations were found during the geometry generation due to the low quality of T1-weighted MR images and to the lack of T2-weighted MRI and computerized tomography (CT) scan. Also, a low control on the mesh generation process led to an excessive element density and tetrahedral elements concentration. A large amount of time was spent on the segmentation process having to use a wide range of methods with increasing user interaction. This has led to a low level of repeatability of the process. Several evaluations were made during this work, such as on original data, geometry result, mesh and simulations result. A correlation was found between original data (i.e. MRI, CT-scan) quality and simulation result accuracy.

**Key words:** Finite Element, Rat brain, MRI segmentation, medical imaging, animal simulation.



# Contents

ABSTRACT	I
CONTENTS	III
PREFACE	V
ACKNOWLEDGEMENTS	V
NOTATIONS	VI
INTRODUCTION	VII
<b>1. Background</b>	<b>1</b>
1.1 Anatomy	1
1.2 Images data Acquisition	3
1.3 Image processing	5
1.4 Previous Research	7
1.5 Previous Model Limitations	9
<b>2. AIM OF THE STUDY</b>	<b>10</b>
<b>3. MATERIALS</b>	<b>10</b>
<b>4. METHODS</b>	<b>11</b>
4.1 Evaluation of appropriate software	12
4.2 Method to evaluate segmentation performance And Image accuracy	12
4.3 Methodology used to get the FE model	15
4.4 Pre-Processing Data	16
4.4.1 Contrast enhancements on the original MR Images	16
4.4.2 Noise filtering	17
4.5 Segmentation process	18
4.5.1 Full-Automated Segmentation	18
4.5.2 Semi-Automated Segmentation	19
4.5.3 Refinement process	20
4.6 Problems and Limitations	21
4.7 Mesh generation	22
4.7.1 Pre-smoothing operation	22
4.7.2 Elements density reduction	23
4.7.3 Meshing criteria (SFE)	24
4.7.4 Mesh refinement operation	25

4.8 Materials and Property assignment.....	27
<b>5. RESULTS.....</b>	<b>30</b>
5.1 MR Images analysis.....	30
5.2 Geometry Results.....	32
5.2.1 Full/Automated Segmentation Results.....	32
5.2.2 Semi/Automated Segmentation Results.....	36
5.2.3 Final Geometry Results.....	40
5.3 Geometry Accuracy evaluation.....	49
5.4 Mesh Results.....	53
5.4.1 Elements density reduction results.....	53
5.4.2 Final Mesh Results.....	55
5.5 Mesh Quality.....	57
5.5.1 SFE Algorithm Limitations.....	57
5.5.2 Mesh Quality analysis.....	58
5.6 FEM Reference Analysis.....	59
<b>6. DISCUSSION.....</b>	<b>62</b>
6.1 Data Analysis.....	62
6.2 Final Geometry evaluation.....	63
6.3 Mesh results evaluation.....	65
6.4 FEM results evaluation.....	67
<b>7. CONCLUSIONS.....</b>	<b>68</b>
<b>8. FUTURE WORK.....</b>	<b>69</b>
<b>9. REFERENCES.....</b>	<b>70</b>

## **Preface**

During this thesis an animal FE model was developed and the relative methodology to operate was presented looking for as high as possible level of repeatability. This will hopefully also represent a first guide line on how to proceed on the development of a FE brain model starting from medical imaging.

## **Acknowledgements**

I would like to thank *Karin Brolin* for her expertise and guidance in finite element method and *Johan Davidsson* for his guidance during this thesis work. A special thank to *Mats Svensson* for give me the opportunity to write my thesis at SAFER and *Manuel Mendoza* for his extra-job and guidance during the writing of the final report.

Göteborg, 2010  
Gianfranco Ramirez

## Notations

<i>Beta APP</i>	beta-amyloid precursor protein, used to trace damage to the axons
<i>CT-scan</i>	Computed tomography scan
<i>DAI</i>	Diffuse Axonal Injury
<i>FE</i>	Finite Element
<i>LS-Dyna</i>	Finite element software from Livermore Software Technology Corporation
<i>MRI</i>	Magnetic resonance imaging
<i>TBI</i>	Traumatic brain injury
<i>ROI</i>	Region of interest
<i>VOI</i>	Volume of interest

# Introduction

Head injuries are still the leading cause of death in motor vehicle accidents. Traumatic brain injury (TBI) occurs when an external force traumatically injures the brain. TBI can be classified based on severity, mechanism (closed or penetrating head injury), or other features. *Head injury* usually refers to TBI, but is a broader category because it can involve damage to structures other than the brain, such as the scalp and skull. TBI is a major cause of death and disability worldwide, especially in children and young adults. It constitutes a significant portion of all injuries occurring as a result of automotive, sports and domestic accidents. Brain trauma can be caused by a direct impact or by acceleration alone. In addition to the damage caused at the moment of injury, brain trauma may cause *secondary injury*, generally a variety of events that take place in the minutes and days following the injury. These processes are usually associated with blood vessels failure, such as contusion and hemorrhage. Intracranial bleeding often results in a grooving mass of clotting blood that, if not immediately treated, may result in severe secondary damage and death due to increasing intracranial pressure and distortion of the brain.

Besides, brain can suffer from *diffuse axonal injuries* (DAI) with consequences on the general health of the complete body. The diffuse axonal injury is categorized as a diffuse brain damage, i.e. an injury that occurs over a wider area inside the brain; specifically the DAI describes disruption to the axons in the cerebral hemispheres.

The mechanisms of such traumatic brain injuries and head injuries in general have not yet been fully established in spite of a great amount of work on it. A powerful used tool to identify injury mechanisms is the *finite element method* (FEM) The study consist in a correlation between real world observed brain injuries and calculated results by using FE model, such as brain pressure or Von Mises stress.

An important part when using FE models involves the validation of the models. Animals are used in order to have a high number of experimental data about TBI mechanism and to validate animal brain FE models. After that, opportune scaling laws are applied to use the animal results in human study. In fact, using an animal can allow obtaining well defined mechanical loading conditions of the head. Thus, it can become easy to control the impact on the head.

Nevertheless, the internal dynamic response of the brain in such experimental studies is hard to measure in vivo, especially if the considered animal is of small size.

Nowadays, living animals are widely used in different labs to study TBI. In many cases, the rat's head is submitted to either linear or angular acceleration.

Previous research on this field was made by *Baumgartner D. et al* (2009). A simple FEM of the rat's head was developed and the experimental data were provided by the experiment done by *Davidsson J. et al* (2009) in which the diffuse brain injuries (DAI) from rotation was investigated in living rats.

The limitation of this model was related to the results obtained from the simulation were not able to predict the *Diffuse Injuries* (DAI).

Thus, a more detailed rat brain FE model was required in order to improve the number of brain regions. In this way it would be possible to perform a reference simulation by

assigning a defined stiffness value for each brain region and could be seen if this new rat brain FE model is able to predict the Diffuse Axonal Injuries.

This thesis describes the method used to obtain a detailed rat brain FE model from medical images. The validation of this model will not be treated in this thesis, but it is the object of study in the *Hultman J.(2010)* by a comparison between simulation results and visual identification of injured axons concentration in appropriate statistical maps.

# 1. Background

## 1.1 Anatomy

Before starting the development process of the rat brain FE model it is necessary to identify the essential brain parts in which we are focus in this work. Therefore, knowledge about the rat brain anatomy is needed. This information was provided through a detailed rat brain atlas by *Paxinos G. et al (2007)*.

The main rat brain regions treated in this work are: the Neocortex, the Corpus Callosum, the Caudate Putamen, the Hippocampus, the Culliculi, the Cerebellum, the Brain stem, the Olfactory Bulb and the Ventricles. Additionally, the Skull and the Brain-Skull interface are needed to complete the rat head FE model. In this part the fundamentals about several rat brain regions treated in this thesis are presented.

### *Neocortex*

The Neocortex is a thin layered structure surrounding rat brain. It is the outer layer of the cerebral hemispheres, and made up of six layers. It is the most divergent part across mammalian species. It is involved in higher functions such as sensory perception, generation of motor commands, spatial reasoning, and conscious thought, in humans, language. "Cerebral cortex" is almost synonymously used as neocortex.

### *Corpus Callosum*

The corpus callosum is a structure of the rat brain in the longitudinal fissure that connects the left and right cerebral hemispheres. It facilitates communication between the two hemispheres. It is the largest white matter structure in the brain, consisting of 200-250 million contra lateral axonal projections.

It is a wide, flat bundle of axons under the cortex. Much of the inter-hemispheric communication in the brain is conducted across the corpus Callosum.

### *Hippocampus*

The hippocampus is a bilateral structure sandwiched between the cerebral cortex and the thalamus. It is a major component of the brains of humans and other mammals.

In rodents, the hippocampus has been studied extensively as part of the brain system responsible for spatial memory and navigation.

## ***Cerebellum***

The cerebellum is a lobed structure located near the base of the brain that is primarily involved with the coordination of bodily movement and the development and recollection of physical skills, such as bike riding. Recently the cerebellum is receiving particular attention. Where the cerebellum was regarded as the neural structure involved in the co-ordination of motor activity, recent clinical and experimental reports suggest that the cerebellum might also be involved in other mechanisms.

## ***Ventricles***

Ventricular system of rat was like “Y” in shape, similar to human .Basically, the lateral ventricles were the first and second ventricles. They were connected to the third ventricle. Continuing lengthwise, the cerebral aqueduct of the midbrain opened into the fourth ventricle. The fourth ventricle occupied the space dorsal to the medulla and ventral to the cerebellum. It can be said that rat ventricular system was similar to human’s one.

## ***Brain stem***

The brainstem is the lower part of the brain, adjoining and structurally continuous with the spinal cord. The brain stem provides the main motor and sensory innervations to the face and neck via the cranial nerves. Though small, this is an extremely important part of the brain as the nerve connections of the motor and sensory systems from the main part of the brain to the rest of the body pass through the brain stem. The brain stem also plays an important role in the regulation of cardiac and respiratory function. It also regulates the central nervous system, and is pivotal in maintaining consciousness and regulating the sleep cycle.

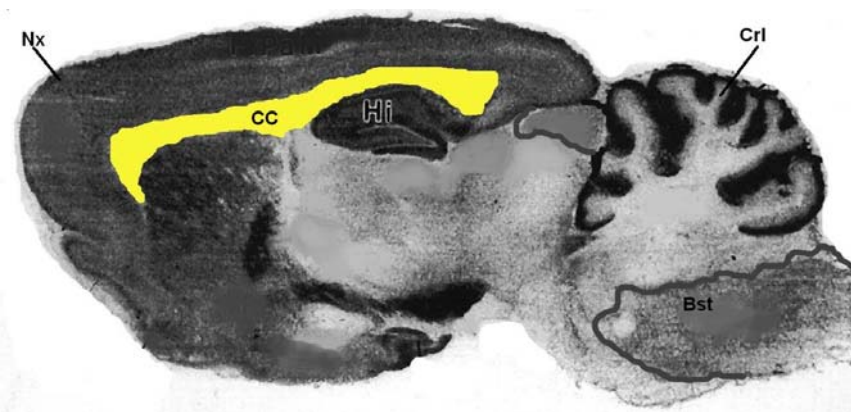


*Figure 1: Cross section along on the sagittal plane. It is possible to notice the location of different rat brain region treated in this work as: Corpus callosum (CC), Neocortex (Nx), Hippocampus (Hi), Cerebellum (Crl) and Brain stem (Bst).*

## 1.2. Images data Acquisition

### 1.2.1. Magnetic Resonance Imaging and CT scans

Magnetic resonance imaging (MRI) is a non-invasive method used to render images of the inside of an object. The typical MRI examination consists of several sequences, each of which is chosen to provide a particular type of information about the subject tissues by using the appropriate contrast mechanism.

A computed tomography (CT) scanner uses X-rays, to acquire its images, making it a good tool for examining tissue composed of elements of a relatively higher density than the tissue surrounding them, such as bone and calcifications within the body, or of structures (vessels, bowel) which have been artificially enhanced with contrast agents.

Unlike CT, which uses only X-ray attenuation to generate image contrast, MRI has a long list of properties that may be used to generate image contrast. By variation of scanning parameters, tissue contrast can be altered and enhanced in various ways to detect different features. MRI is best suited for non-calcified tissue.

While CT provides good spatial resolution (the ability to distinguish two structures an arbitrarily small distance from each other as separate), MRI provides comparable resolution with even better contrast resolution (the ability to distinguish the differences between two arbitrarily similar but not identical tissues).

Another point of difference between MRI and CT is the image clarity and the impact on the *segmentation* process.

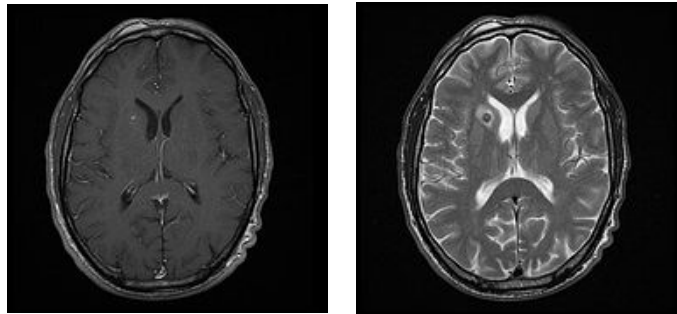
In order to obtain a good segmentation some very simple threshold based tools can be used with CT-scan images. However it is not efficient at distinguishing between different soft tissues.

In MRI, in terms of image quality, is ideal to visually distinguish soft tissues, but objects must contain hydrogen molecules (i.e. water). Segmentation can be threshold based in some cases, even if MRI images often suffer from signal attenuation and/or noise on the borders of the region of interest.

However it is quite frequent to see different objects easily distinguished visually only by texture. In this case, manual segmentation may be required.

### 1.2.2 Contrast mechanism in MRI

There are many contrast mechanisms that one can use in MRI. The key word here is *weighted*. In this context, *weighting* simply means the amount of contribution made to the image contrast associated with the difference between tissues on the basis of the parameter of interest (PD, T1, or T2). This weighting is accomplished by the selection of the timing parameters of the pulse sequence such as TR (repetition Time) and the TE (echo time). TR primarily controls the amount of T1-weighting, whereas TE primarily controls the amount of T2-weighting, *Prince J.L. et al (2005)*.



**A:  $T_1$ -weighting**

**B:  $T_2$ -weighting**

*Figure 1.1 : The different parameter weightings discussed.*

### **$T_1$ -weighted MRI**

In the brain  $T_1$ -weighted scans provide good gray matter/white matter contrast, fat is high signal intensity and cerebrospinal fluid (CSF) low signal intensity (Figure 1.1 A).

This is one of the basic types of MR contrast and is a commonly run clinical scan.  $T_1$ -weighted scans use short TE and short TR. The  $T_1$ -weighting can be increased in order to improve the contrast. There is no exact “best” TR, but rather a range to produce  $T_1$ -weighted images usually between 400 and 550 msec. The range depends on the tissues being imaged as well as the field strength of the MR system. Often, one selects the shortest TE possible in order to run this scan in the faster way.

### **$T_2$ -weighted MRI**

They are particularly well suited to edema as they are sensitive to water content. Water- and fluid-containing tissues are bright and fat-containing tissues are dark. The reverse is true for  $T_1$ -weighted images (Figure 1.1 B).

$T_2$ -weighted scans use a long TE (usually 80 to 120 ms) and long TR (usually 2500 ms or higher). Heavily  $T_2$ -weighted images find application for visualization of fluid such as CSF. CSF is high signal intensity and the gray matter-white matter signal intensity ratio is reversed compared to that of  $T_1$ -weighted images.

In this work both of these methods are needed in order to have an appropriate definition of the different brain regions and CSF.

## 1.3 Image processing

In mechanical engineering, the typical used method to describe volumes is Computer Aided Design (CAD) approach through splines, triangles, etc.

In recent years, new methods were developed and used to generate high-fidelity models constructed from data obtained from three-dimensional imaging modalities (i.e. CT and MRI). Anyway, for a wide range of objects, such as biological structures, no CAD description is available; the simplest approach to obtaining a topological model of these structures is using an automated method for three dimensional volume or surface acquisition. By using these methods we then obtain a partitioning of the space in bricks. These bricks are called voxels (volumetric pixels). A new different approach is able to skip the conversion to a CAD description and mesh directly from bitmapped data which results in a far more robust and automated approach.

However, most approaches to converting three-dimensional images into meshes for use in FE analysis necessitate significant user interaction and often still involve some appreciable simplification of the model geometry *P. G. Young et al (2008)*.

### 1.3.1 Volume Images

A volume image can be seen as a 3D matrix composed of 3D pixels, also called voxels, in each direction (X, Y, and Z). Usually, the slices are oriented in the XY direction, thus the number of pixels in the Z direction is also often called *Number of Slices (or slice thickness)*. The *spacing* is the size of each voxel in each direction (X, Y and Z), in real units (Figure 1.2).

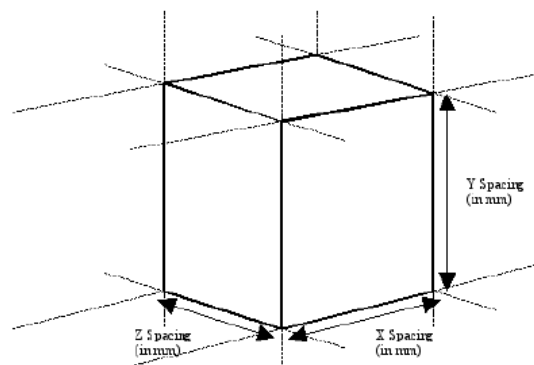


Figure 1.2: Single voxel representation

Instead of X, Y and Z spacing, the terms in-plane resolution and slice to slice distance can also be used, and they are equivalent. The spacing can be different in X, Y and Z but must be constant in each direction. In volume images, those voxels (or brick elements) are positioned on a rigid 3D grid.

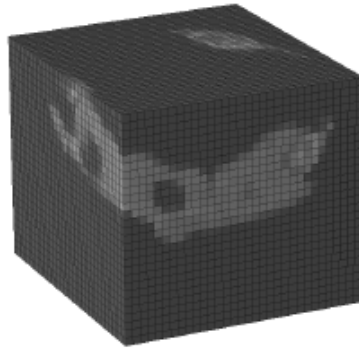


Figure 1.3: A volume image can be seen as a 3D table composed by voxels.

The data extent can be expressed in number of pixels/voxels or in real units (mm).

Although structured, the grid mentioned previously need not be isotropic. We define the spacing as being the edge length of each voxel. Spacing is defined in each direction (X, Y and Z) and it is the same throughout the volume.

We use the term Background data to refer to *Grayscale* data (e.g. CT, MRI data).

The image processing is called *Segmentation* which working on the Background data will then generated one or more volumes (binary volumes) that are called *Masks* and that define how an object fills the space. Ideally, each object of interest (ROI) should be represented by a mask. These masks can be worked on, modified and filtered, until the user is satisfied with them and decides that they should be converted into a mesh. For a binary mask (all masks are binary containing only 0 and 1) a value of 1 for a pixel means that the pixel belongs to the object the mask is representing (inside). A value of 0 means that the pixel does not belong to the object (outside).

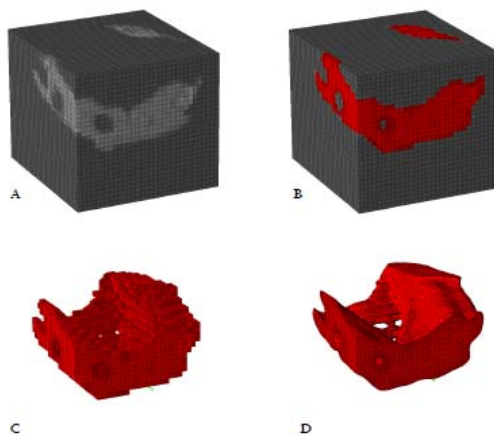


Figure 1.4: shows an example of background data (grayscale) from which a mask has been created as part of the segmentation process from scanned data to STL (or FEM) model in four basic steps.

- A) *Volume image*: Data from three-dimensional imaging modalities generally consist of a regular Cartesian grid of grayscale data representing the relative signal strength throughout the scanned volume obtained from the imaging modality. The picture (a) shows how it is possible to detect the *volume of interest* (VOI) from the rest of background.
- B) *Segmented image*: The most basic step that must be carried out is *segmentation*: that is the identification of volumes of interest (VOI) within the image by classification of voxels into appropriate groups (bone, fat, muscle, etc.), through various techniques ranging from manual to automated approaches.
- C) *Segmented mask isolated*: The VOI was isolated by the background and the result obtained is the original voxel mesh created by brick elements only.
- D) *Smoothed STL generated*: We have a rendered view of surface mesh obtained by the mesh generator from the original mask, through a smoothing operation.

## 1.4 Previous Research

A previous research on that study was made by *Baumgartner D. et al (2009)*. A simple FEM of the rat's head was developed and only four brain parts the brain/skull interface and skull were included.

The development of the FEM needed three main stages. The first one was obtaining the geometry of the different anatomical head components, such as, the skull and brain geometry, which was based on CT-scan and magnetic resonance (MRI) images respectively. The other stages consisted in the meshing of the geometry and eventually in the definition of the materials properties. An analysis of the rat's head FEM was performed by applying an angular acceleration to the rat's head in the sagittal plane at its centre of mass. That acceleration relies on the experimental study made by *Davidsson J. et al (2009)*. In this FEM analysis, brain pressure and brain Von Mises stress were computed and compared to the observed injuries in order to elucidate potential brain injury mechanisms.

The geometry of the rat's head was obtained from CT-scan and MRI pictures and modeled with Scan2Mesh (ALTAIR HYPERWORKS 9.0 © software). Through this software was possible to carry out a simple segmentation process, because only four brain regions were required in this rat brain FEM.

The brain segmentation was performed on T1-weighted MRI images with a fairly low resolution, but it was enough to get a simple and less detailed brain geometry.

The mesh generation was realized by using Hypermesh software (by ALTAIR HYPERWORKS 9.0 ©). The main anatomical features modeled were: skull, brain/skull interface (which includes the cerebral spinal fluid and the meninges), olfactory bulbs, cerebrum, cerebellum and brain stem.

The finite element mesh was continuous. The average size of the edges of an element was about 0.45 mm. The skull was simulated with one layer of shell elements whereas the other anatomical components were meshed in hexahedral elements. Overall, the

FEM of the rat head was composed by 17,972 hexahedral elements and 3,220 shell elements. The mechanical behavior of the skull and of the brain/skull interface was assumed to be linear elastic, isotropic and homogenous.

The experimental data that was chosen for the reference simulation and to lead the parametric study was provided by Davidsson et al. (2009). It corresponds to a mechanical loading of the rat's head for which light DAI were diagnosed. In fact, for higher levels of angular acceleration heavy DAI were observed whereas for lower levels no injuries were sustained.

Thus, the velocity that is applied to the rat's head in the sagittal plane at its center of mass is illustrated in Figure 1.5.

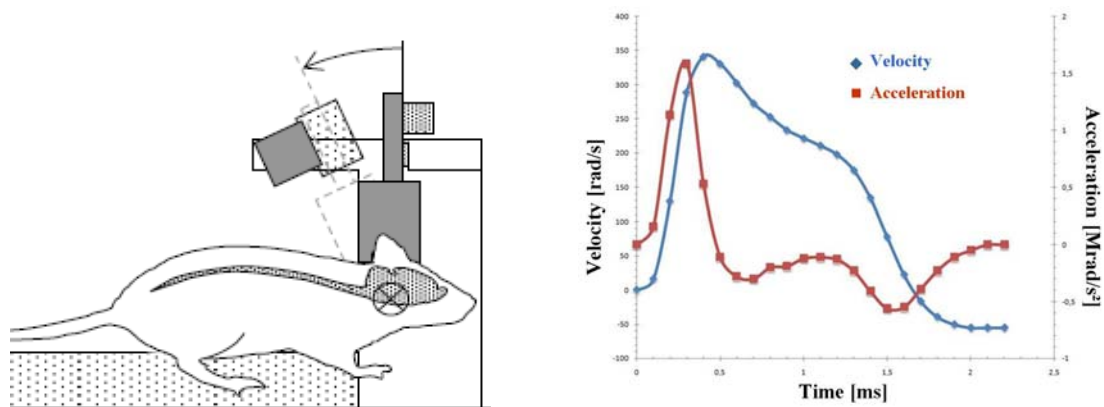


*Figure 1.5: Angular acceleration and velocity that are applied to the rat's head FEM at its centre of mass in the sagittal plane.*

In that analysis of the rat's head FEM brain pressure and Von Mises stress were recorded in terms of time history and anatomical distribution in the cerebrum, in the upper and lower olfactory bulbs, in the brain stem and cerebellum.

## 1.5 Previous Model Limitations

From the reference simulation results was possible to see as this FEM is able to predict *Focal Injuries* because high pressure concentration in the simulation results correspond to part of the brain with high damage in which hemorrhages were visual.

The limitation of this model refers to the *Diffuse Injuries* (DAI). The results obtained from the reference simulation were not able to predict this kind of injuries. This could be explained that the stiffness in the rat brain is not uniform and then local deformation may occur in the border between the corpus callosum and surrounding tissue and in the lower part of the hippocampus, as showed in the picture below.

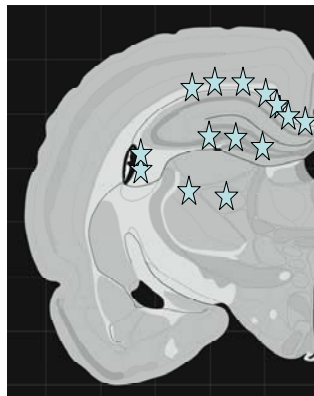


Figure 1.7: Stars indicating localization of  $\beta$ -APP-positive axons in a schematics of the middle coronal section of the rat brain.

In this rat brain FEM these parts were not generated because they were included in one part only called cerebrum as showed in figure 1.8.

It should be of interest to develop a more detailed model by dividing the cerebrum part in several regions, such as corpus callosum and surrounding tissues, with different material properties in order to obtain simulation results as close as possible to the experimental data.

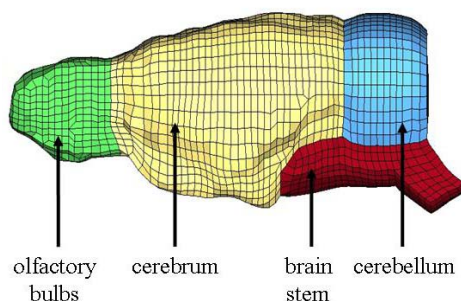


Figure 1.8: Baumgartner's FE Model generated with four brain part only. Cerebrum part includes several internal brain regions.

## 2. Aim of the study

In this study, a finite element model of the rats will be developed to improve the knowledge on traumatic brain injuries. A 3D digital model of the live rat brain based on magnetic resonance microscopy (MRM) is presented.

More specifically, the aims of the study are:

- To get the rat brain Geometry from MR Images by evaluating appropriate software and developing a repeatable methodology.
- To get the Mesh from the Geometry, thus, to analyze and to improve the mesh quality.
- To evaluate the FE Model accuracy

This study shows how powerful numerical tools can be to better understand injury mechanisms and thus to conceive protection devices against extreme mechanical loadings of the human head.

## 3. Materials

The material used to carry out this thesis work includes various components.

At the beginning a set of MR images were provided by *Karolinska Institutet* (Stockholm) as T1-weighted MRI. After a literature review including a previous similar study done by *Baumgartner D. (2009)* two different software were used in order to see which one was the most appropriate to get the level of detail required for this thesis work.

Scan 2 Mesh (ALTAIR HYPERWORKS 9.0 © software) was used at the beginning, but it was not powerful enough to get the correct brain geometry, therefore Scan IP + Scan FE (Simpleware® software) was used to carry out the 3D geometry and the mesh from the MR images.

During the segmentation process a rat brain atlas (*G. Paxinos and C. Watson 2007*) was used in order to identify the different rat brain regions and their location in the space.

Several operations and mesh analysis were performed with Hypermesh (ALTAIR HYPERWORKS 9.0 © software). The simulation of this FE model was calculated with LS-DYNA code in order to simulate the experiment carried out by *Davidsson et al (2009)*.

## 4. Methods

In this chapter several methods are presented, the goal in this framework is to develop a repeatable methodology to generate a FE model from MRI data. This can be achieved by well defining the different operations and sub-operations required to perform an acceptable segmentation process, this means to get a good geometry result and the final mesh generation. Another important goal of this work is by founding a method to evaluate the different results obtained during this process, such as MR Image quality, performance of the segmentation process, mesh elements quality and accuracy of FEM results in order to reduce the birth and diffusion of error.

Overall, this work was carried out in several main parts as presented below.

- The first part requires a deep literature survey in order to have sufficient information on the location and geometry of the various brain regions. This step can be called "*a priori knowledge*" and could be done by the help of a detailed statistical rat brain Atlas.
- The second part involves choosing dedicated software, which can ensure a good segmentation process performance, in order to get an accurate geometry result. After that user training would also be required, to make best use of this software.
- In the third part we propose to develop a repeatable algorithm to carry out the final FE rat brain model. This is the most important part of this work in which we try to improve as much as possible the repeatability of the methodology used.

This part is divided in three main operations, as shows the Figure 4.1.

The first operation works on the grayscale of the original data by using data operations and image filtering in order to remove the noise from the background. This operation is also called "*Pre-processing of data*" operation.

The second operation is the *segmentation* operation in order to extract the different Volumes of Interest (VOI or "Masks") from the background and then improve their surface quality (smoothing) by using several filters.

- The last operation after the segmentation process is exporting the 3D geometry model, this leads to the mesh generation, thus the final FE model.

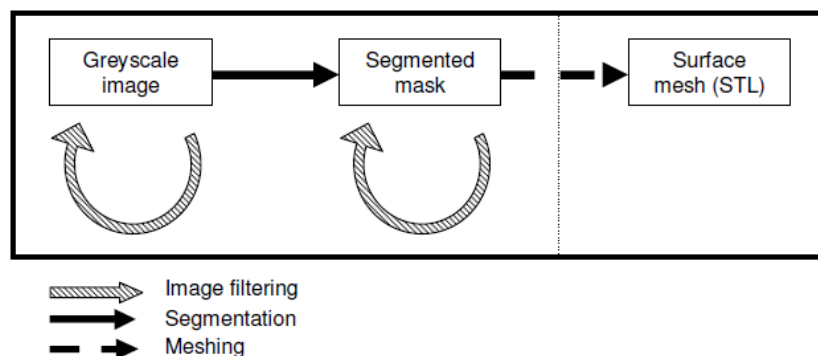


Figure 4.1. Main operations to obtain a FE model from MR (or CT-scan) Images.

Once the FEM will be carried out, the following operations are: the materials, property and load condition assignment in order to perform several simulations with LS-DYNA code and evaluate the accuracy of the FE model results.

## 4.1 Evaluation of appropriate software

In this part a valuation of two different software was performed, the goal of this operation was to found the basic tools needed to be able to perform a good segmentation process, such as, Images information, user training, helping support and more specific tools for the segmentation. It is very important to choose a software in which a deep training is no required in order to affect as low as possible the repeatability of the segmentation process. In this case the software used for the comparison were Scan 2 Mesh (Altair HyperWorks 9.0 © software) and Scan IP + Scan FE (SIMPLEWARE © software) in order to value which one of these is able to perform a good segmentation and to provide the best results.

After an accurate comparison between these software Scan IP (SIMPLEWARE ©) was chose. The best solution in order to obtain an accurate geometry and mesh result is working with Scan IP, because it's more powerful than Scan2Mesh with the semi-automated and manual method. It is more appropriate to work on MRI image, because it offers a lot of different tools filters and edit functions useful to get the detail level required in the rat brain FE model treated during this thesis.

Scan2Mesh could be a good working tool only by using a threshold function with CT-scan Images, because in this kind of images a strong contrast should be provided.

## 4.2 Method to evaluate segmentation performance and Image accuracy

A good tool to control the grayscale of the region of interest (ROI), in which we are working on, is the *histogram tool*. This means to be able to valuate the original images accuracy and the segmentation performance by using the histogram belonging to the background and segmented ROIs (or Masks).

To better understand this histogram tool we should consider some concepts of statistical theory, about the normal distribution, mean and standard deviation.

The picture 4.2 shows as the standard deviation means how much variation there is from the "average" (mean). A low standard deviation indicates that the data points tend to be very close to the *mean*, whereas high standard deviation indicates that the data are spread out over a large range of values.

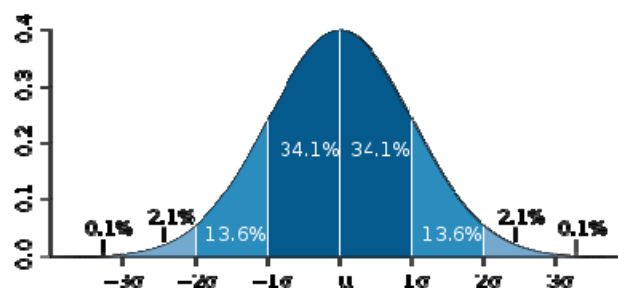


Figure 4.2. Example of Standard deviation (34.1% in this case). In this graph  $\mu$  is the mean and  $\pm\sigma$  is the standard deviation.

From the original data we could be able to identify the different regions of interest as peak in the Histogram of the images background. In the figure listed below (Fig. 4.3) an example of histogram of human brain MRI is showed, and it is possible to see as the grayscale of each region of interest (skull, CSF, grey matter and white matter) are well defined and set to the four top peaks of the histogram.

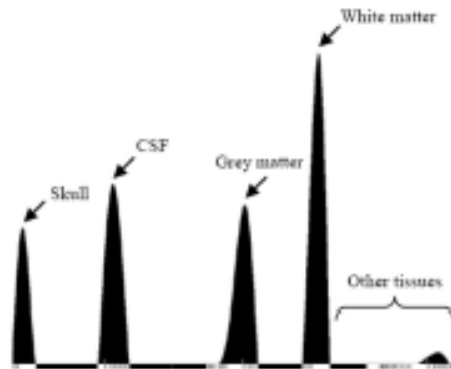


Figure 4.3: Histogram of Human brain MRI from BrainWeb

As showed in figure 4.4, the histogram tool allows to see the frequency of the grey scale value belonging to the images background. The graph shows the *frequency of occurrence* of pixels with the same grayscale intensity value into a range between 0 and 255. The grey scale at the top of the graph shows the color that the corresponding background value is rendered in the slice views.

In our case during the segmentation process we have pay attention to the histogram tool, in order to have the histogram with a standard deviation as low as possible, so all the pixel tend to be close to the main pixel intensity value of the region of interest.

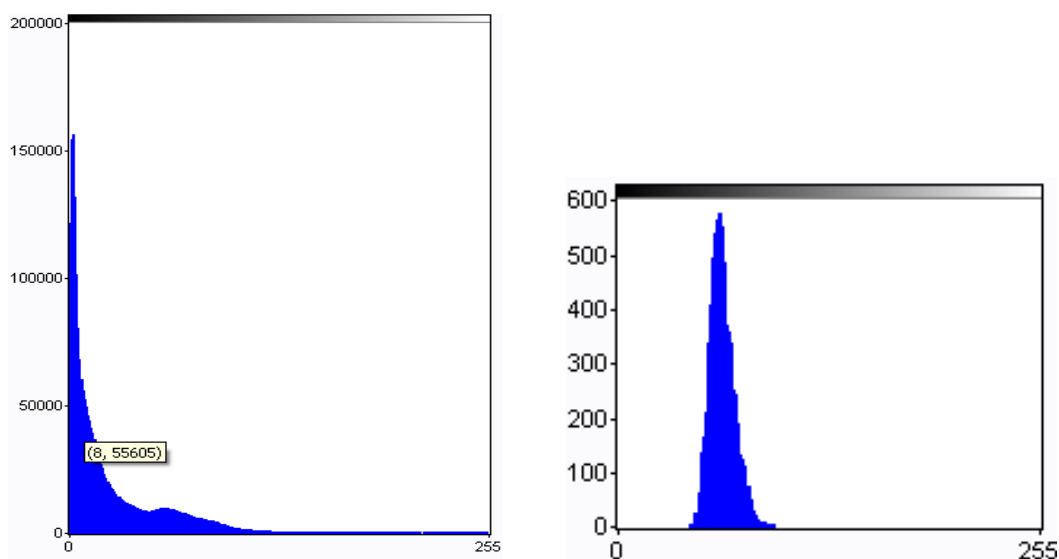


Figure 4.4: Grayscale of background from current data (right) and Grayscale of a single region (Mask) from current data (left).

The histogram of the background (fig.4.4, left) shows as, across the series of MRI images provided in this work, the maximum value of *frequency of occurrence* of pixel intensity decreases rapidly from  $15.0e+04$  to fluctuate around a value of  $1.0e+04$ .

This means that most of the massively images are quite dark, with a fairly uniform grayscale of the pixels; this also means images with low contrast.

The histogram on the right shows the grayscale values of a single *Mask* of a region of interest (ROI) that in our case is one organ, which presents a mean intensity value of 63 and a standard deviation of 8. It is possible to see as for the mean intensity value the *frequency of occurrence* value is close to 600. This means that the ideal solution to work with this software, by using a Full-automated (Threshold) or Semi-automated (*Confidence connected region growing*) approach, would be only a single grayscale value for each ROI, and this would be represented in the histogram with a single vertical line joining the maximum value of *frequency of occurrence* of pixel (or voxel) with the corresponding grayscale values. This kind of solution could exist in the CT-scan images.

Actually, this solution is not possible with the MR images, but it is possible to obtain intervals as closely as possible (low standard deviation) for each ROI and with *frequency of occurrence* values of pixels on average higher into the considered range.

To evaluate original MRI and segmentation results two important observations are done:

- *On the background:* a significant difference ( $\Delta$ ) in mean intensity values is required between each ROI and the neighboring ones. This also means having a good image contrast in the original data.
- *On the Mask:* the standard deviation of each ROI should be as low as possible, with the pixels intensity values as close as possible to the mean value.

A good segmentation result will be the Mask having a grayscale with a low standard deviation and with its means intensity value as much different as possible from that of surrounding regions.

### 4.3 Methodology used to get the FE Model

The methodology used to get the FE model can be mainly divided in two different parts to well understand the different sub-operations in which they are divided. In the first part of this algorithm the different operations to get the geometry were founded and the second part was used to well define the different operations to generate the mesh.

#### Method used to get the 3D Geometry

In this part of the study the method used to get the 3D Geometry is presented.

*Table 4.1) The main two operations and several sub-operations used in this method are listed in the table below.*

<b>Method to get the 3D Geometry</b>			
<b>N</b>	<b>Operation</b>	<b>N</b>	<b>Sub-Operations</b>
1	Pre-Processing Data	1.1	CT/MR Images analyses
		1.2	Contrast enhancement
		1.3	Noise filtering
2	Segmentation Process	2.1	Fully-Automated Segmentation
		2.2	Semi-Automated Segmentation
		2.3	Refinement process

#### Method used to get the mesh

Once the geometry was obtained, the following step was used to obtain the complete mesh of the FE model, this was achieved with several software: first with ScanIP (simpleware®), then ScanFE (simpleware®), and then with HyperMesh (ALTAIR HYPERWORKS 9.0 ©).

*Table 4.2) In each one of this software several operations were performed as listed in the table below.*

<b>Method to get the Mesh</b>		
<b>n</b>	<b>Operation</b>	<b>Software</b>
1	Pre-smoothing	Scan IP
2	Element density reduction	
3	Mesh refinement	Scan FE
4	Skull part design	HyperMesh

## 4.4 Pre-processing Data

This operation is one of the most important in this process and it was divided in three different sub-operations: a) Initial data analysis b) Contrast enhancement c) Noise filtering. The first sub-operation is the most important because it leads to a correct evaluation of the initial data (MR Images) in order to choose the correct type of segmentation process (Automated, Semi-automated or Manual) and to evaluate which part in the original images it possible to segment or not. This sub-operation will performed through a visual analysis followed by a much more accurate study by using the *histogram tool method*, as mentioned previously.

The last two sub-operations are used to improve the initial images quality by improving the image contrast and removing the noise from the background through filtering operations. These operation will performed by using Scan IP software (Simpleware ©).

### 4.4.1 Contrast enhancements on the original MR Images

By using the window and level settings during the MRI import we can adjust the contrast between the brain and surrounding tissues, as showed in Figure 4.5.

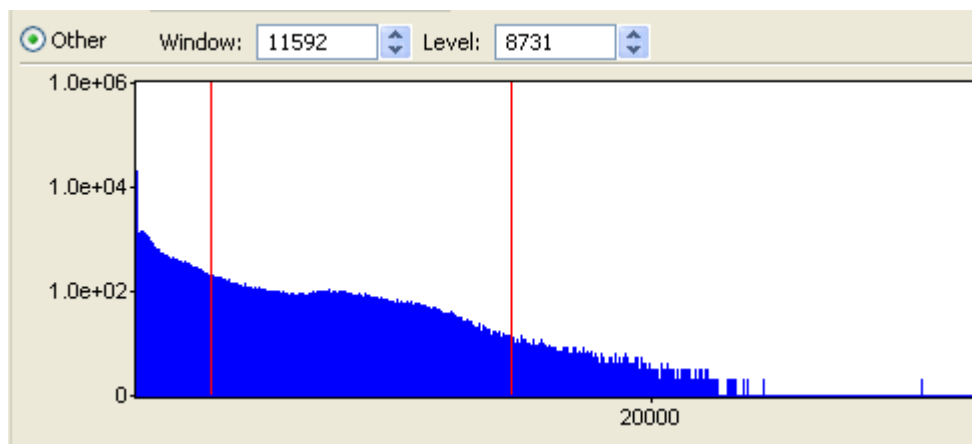


Figure 4.5. Window and level settings from current MR Images

With Scan IP it might be possible to use the current images to get the model required, it just depends whether the regions of interest are visible in the image with enough contrast to distinguish them. One way of generating more contrast is during the Dicom import procedure, to calculate the histogram which will allow adjusting the window and level settings. We can also import the same set of images several times with different window and level.

#### 4.4.2 Noise filtering

In Scan IP this kind of filter is called *Recursive Gaussian filter*. The visual effect of this technique is a smooth blur resembling that of viewing the image through a translucent screen as showed in Figure 4.6.

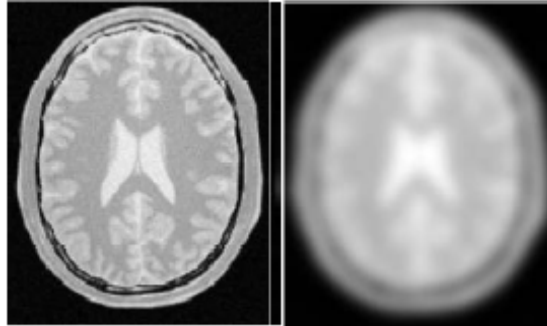


Figure 4.6. Human head MRI before (left) and after (right) applying the recursive Gaussian filter.

In our case, this kind of operation was not performed due to the low image quality provided. By attempts was possible to see that once applied the filter is no more possible to recognize the boundaries between an internal organ and another. This is a classic operation that precedes the *fully automatic segmentation* by using the *thresholding* function.

Unfortunately, we cannot use this kind of segmentation with the images we have. In fact, the only possible result would be to obtain the geometry of the whole brain as a single part. Instead with this work we need to get more than 8 different regions within the brain.

We use this filter only in the final steps in order to drop the geometry detail level, thus improve the smoothing operation.

## 4.5 Segmentation process

Segmentation of medical images is an important area of active interest and the techniques available extend in a wide range from manually ‘painting’ voxels through to use of different methods to identify contours.

Clearly, the accuracy of any resultant model is largely dependent on the accuracy of the initial segmentation and this is a function not just of the MRI image resolution but a number of other factors including noise and poor contrast between tissues as well as, for semi-automated and manual approaches, inter-operator differences stemming from interpretation of images.

This is the main part of this work, in this operation the 3D brain geometry was carried out by using different kind of segmentation methods in order to reduce as much as possible the operator interaction, thus to have a good repeatability of this process. The first kind of segmentation was made by using a fully-automated approach in order to have the highest repeatability of the process. The last two typology of segmentation requires an increasing amount of user intervention, thus the repeatability is totally affected by the user training with the software used during the segmentation process. In our case this software was Scan IP (Simpleware ©).

The goal in this framework is obtaining the geometry (i.e. STL file) of various brain regions by starting from T1-weighted MRI images; this was carry out by a process called *Segmentation* (or better known as image processing). Segmentation is the process of identifying which object each pixel belongs to. This is why most of the time is spent in this process. In this study a histogram-based segmentation algorithm (HBSA) was used in order to extract the rat head and brain geometry.

The brain MR image was segmented in 10 different regions of interest (ROI), these regions are: the *neocortex*, *hippocampus*, *olfactory bulbs*, *caudate-putamen*, *colliculi (superior and inferior)*, *cerebellum*, *brainstem*, *corpus callosum (external capsule)*, *ventricles*, and *the brain/skull liquid interface (CSF)*. These regions were segmented by using a semi-automated and manual approach.

The results were achieved by using as much as possible the *full automated* and *semi-automated* segmentation approach through the *Thresholding* and *Confidence connected region growing* functions respectively. After that a *masks refinement* process was performed through several manual functions (i.e. Flood Fill, paint/unpaint), different filters (Morphological and Gaussian), and Boolean operations. All of these tools are available with the software used in this work.

### 4.5.1 Full-Automated Segmentation

The results of this operation are strongly dependent from the quality and accuracy of the original MRI images used to extract the geometry. Before start with this operation an accurate analysis of the original data is required. This could be done by using the histogram tool in order to valuate if it is possible to identify the different regions of interest as peak in the histogram, this means that the grayscale of these regions could be well defined.

### ***Threshold function (SIP)***

Threshold selects a window of grayscale values in the middle of which the mean intensity value (or peak) is collocated. It is useful where segmentation can be achieved based on grayscale intensities. Since Scan IP (By Simpleware®) uses a 0-255 range of pixel intensity values, this the way to control the Lower and Upper threshold values in order to split this range in several windows of grayscale each one belonging to a well defined ROI.

### **4.5.2 Semi-Automated Segmentation**

For the work we're going to do, we will use mainly the *Confidence connected region growing* function, after that a *refinement* process will be performed, which includes some adjustments through filtering operations (Morphological and Gaussian) and manual segmentation.

#### ***Confidence connected region growing function***

The user selects a *seed point* which will define the starting region.

For the first iteration, the mean and the standard deviation will be calculated using the pixels around the seed point that are within the “*initial neighborhoods radius*” parameter. Then at each iteration, pixels connected to the region and which *grayscale intensity* (pixel value) lies within the confidence interval are added to the region.

This process is repeated for the specified *Number of iterations* and a *Multiplier* setting of 2.5 would define a confidence interval wide enough to capture 99% of samples in one defined segment.

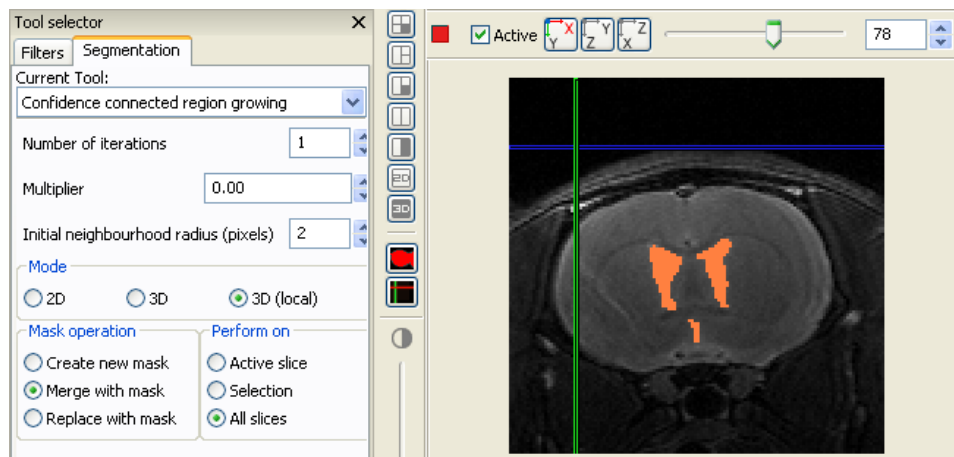


Figure 4.7. Example of segmentation with original MR Images. The orange region indicates the ROI achieved through the segmentation process.

### 4.5.3 Refinement process

In the masks refinement operation, it was quite possible to get the required model by using the current images, it just depends whether the regions of interest (ROI) are visible in the image with enough contrast to distinguish them. This operation was carried out in several different steps (or sub-operations).

- In the first step we try to use as more as possible the *Confidence connected region growing* function in order to improve the initial segmentation.
- After that a combination of manual segmentation (i.e. paint and Flood fill), a morphological *close* filter was used to improve the initial segmentation filling all the holes (empty pixels) and tidying up the edges.
- A third sub-operation was therefore to apply a recursive Gaussian smoothing filter on all brain ROI to smooth the external surface, thus to drop the geometry detail level.

For the rest of the model something similar was performed. The segmentation process was followed by the use of filters to tidy up and smooth the different brain regions.

- Another step involves ensuring the total absence of empty pixels along the interface between the different regions, because when there are lots of *masks* (or ROI) there are no easy ways to automatically fill gaps between masks, and then different ways was used to solve this problem.

Two of them are by using the morphological filters and by using the Booleans operations.

Booleans operations consist in dilate a mask to fill gaps, or use a slightly more complex route: where gaps appear between Masks 'A' and 'B' we could firstly add B to A using a Boolean Union. Then by applying a morphological close filter on the union mask in order to close the holes without affecting the outside surface. Then subtract B from A to separate the masks again. An alternative is to use the paint tool to manually fill the gaps.

- The last step was achieved by trying to simulate the Brain/Skull liquid interface (CSF), which was carry out by using a similar procedure described above. At first by creating a unique mask of the brain, thus expanding it, and then subtracting it all the other masks (or regions) of the brain. The result was an external capsule of the brain; this operation could be called "*Forced segmentation*".

This is not the correct way to get the segmentation of this part, but to get it in the right way T2-weighted images scan are indispensable.

## 4.6 Problems and Limitations

During the segmentation process several limitations were found by working with the *Confidence connected region growing* function on the current MR images.

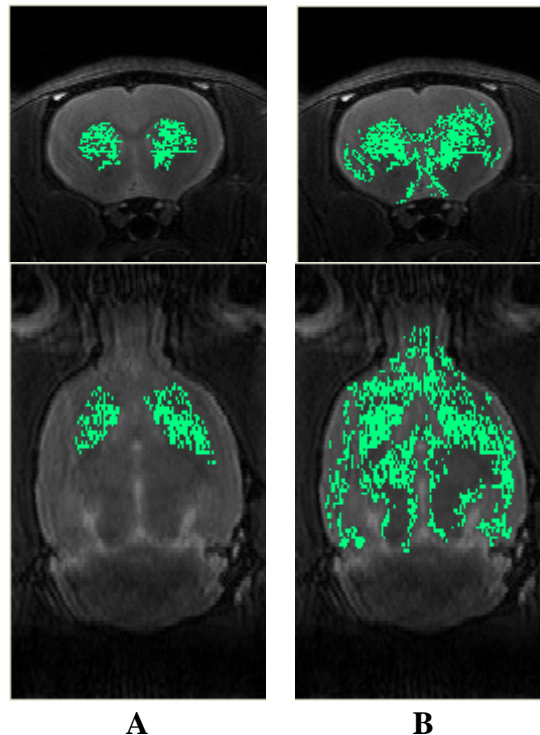


Figure 4.8. Different limitations of the semi-automated segmentation.

The limitations showed in figure 4.8 are the following:

1. Not all of the pixels into the area of interest (ROI) present the same gray scale intensity values of the pixels selected (A).
2. In the same area of interest there are many pixels with the same grayscale value of other areas not of interest (B).

These limitations are closely related to the presence of noise and the low images contrast and resolution. It needs manual fixing on all the images to be able to select all the pixels in the same area; this could be done by using the functions *Paint/Unpaint* and *Flood Fill*, but this means a long time consuming.

By the help from the software technical support, it was concluded that if more details and smaller features are required, a higher resolution scan is needed, also to help with the segmentation (e.g. *threshold* or *Confidence connected region growing*) there should be a visible contrast between the different parts, this means a significant drop in the grayscale.

## 4.7 Mesh Generation

### 4.7.1 Pre-smoothing operation

Before to get the final mesh another preliminary step in Scan IP (Simpleware® software) is needed to better perform the smoothing operation of these elements. This is possible by using an optimal priority position in the Masks list (or Dataset browser) as mentioned below.

Priorities are assigned to masks depending on their position in the Dataset browser. Parts (masks) with higher priority will have their nodes move less, ensuring higher smoothness than parts with lower priorities.

Masks at the top in the Parts for export list have a higher priority than masks situated at the bottom. If an exporting of several masks is needed, we should therefore make sure to have masks for which smoothness is most critical at the top of the list.

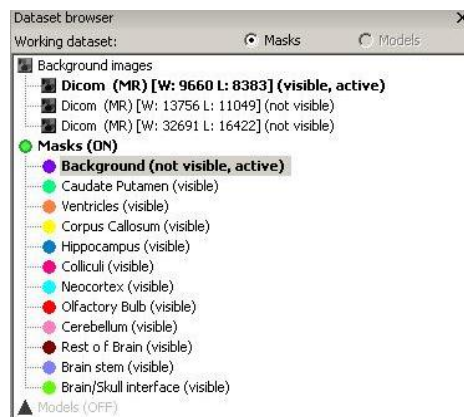


Figure 4.9. Example of masks list

To improve the smoothing between the interfaces it is possible to apply this option during the export from ScanIP and the meshing in ScanFE. Also to smooth where the masks meet on the outer surface of the brain, a method called "*smoothing against the background*" was used. In ScanIP it was created a mask which represents all the brain masks, then this was placed at the top of the list and export to ScanFE. It basically gives the outside space priority for smoothing as showed in figure 4.9.

#### 4.7.2 Elements density reduction

In this operation a decrease in number of element was performed in order to drop the total number of elements. This operation in ScanIP (Simpleware® software) is called “*Data Resample*”. It works on the voxel dimensions (X,Y pixels and slice thickness), the user can change these values in order to found the optimal compromise between elements density and geometry accuracy.

It was used in order to reduce the size of the images by lowering the resolution without modify the object size, even if it may in that case result in loss of features. The sampling rate directly affects the number of elements which are generated in ScanFE (Simpleware® software), because the voxels spacing in the three dimensions changes; this is the primary method to control the mesh density.

To resample the data there are the following steps:

- a) Set the values for X, Y and Z. Y or use *Cubic Resampling* in order to make the values in Y and Z match the X value
- b) Choose a Mask Interpolation method

There are several Interpolation method options that could be sets, in our case the most interesting for this study were the following:

- *Linear*: classic resampling by using a linear interpolation between the neighbors
- *Nearest neighbor*: classic resampling by using the nearest neighbor for interpolation

During this operation, quite long time was spent to find the best combination between fewer elements and best result in terms of geometry accuracy.

After the resampling the linear interpolation technique left holes between the masks, therefore, it is always worth checking for gaps and these can be fixed by painting. If the segmentation is totally conforming (i.e. no empty space between masks) then the mesh will have no holes. The *Nearest neighbor interpolation* method was used in order to avoid gaps along the interface between one region and another.

#### ***Extracting surface and Mesh generation (in SFE)***

After the initial smoothing and element density decrease operations performed in ScanIP, the pre-smoothing option was used for the FE export in Scan FE, in order to preserve volume and topology fairly well 30-50 iterations were used.

In ScanFE, the image data segmented in ScanIP is transformed into a solid meshed model and, reflecting this, we use slightly different terminology within ScanFE to that used in ScanIP, each Mask exported from ScanIP is referred to a separate Part in ScanFE.

### 4.7.3 Meshing criteria

By default, ScanFE (simpleware®) generates an initial mesh consisting only of brick (voxel) elements in which the surfaces of parts are inherently unsmoothed. The meshing operation provides the controls for generating a high-quality smoothed surface mesh on the exterior of each part and for adapting the non-surface interior mesh of parts. The resulting meshes consist in a mixture of tetrahedral and hexahedral elements.

To better understand this meshing operation the four steps of the algorithm used in ScanFE are listed and showed in the figure below:

- a) The initial solid mesh with only brick element is generated by default.
- b) All brick elements are tetrahedralized (split in tetrahedral) in order to smooth the external surface
- c) Where is possible the tetrahedral elements are reconverted into hexahedral, this leads to have a final mixed mesh with tetrahedral elements on the curved surface and hexahedral element away from boundaries with curved surface.
- d) In the last step (optional) an internal adaptation is performed in order to reduce elements density. This is achieved by joining the hexahedral elements together in order to have larger hexahedral elements, thus reducing the total number of elements.

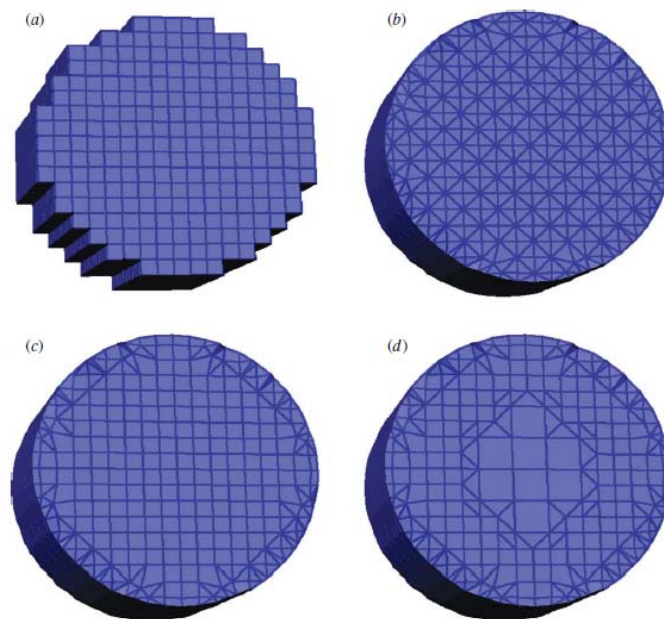


Figure 4.10. The four step used by the SFE algorithm

#### 4.7.4 Mesh refinement

In this operation the geometry was imported in SFE (simpleware®) from SIP in form of voxels (or brick element ), therefore, these elements were converted in a mixed mesh (with hexahedral and tetrahedral elements) through the mesher algorithm of SFE.

Table 4.3) In this part several setting could be done to improve the mesh refinement and to carry out the best result, as listed in the table below.

<b>Parameters setting</b>		
<b>n.</b>	<b>Parameter</b>	<b>Description</b>
<b>1</b>	<i>Mesh type</i>	It is possible to convert the initial brick elements (Voxels) in a smoothed mesh to generate a smoothed surface mesh (hexa/tetra or full tetra) for all parts.
<b>2</b>	<i>Mesh quality</i>	to set the Minimum quality target. During optimization it refers to tetrahedral quality. When reducing the number of tetrahedral, it refers to the quality of the resulting hexahedra.
<b>3</b>	<i>Max iterations</i>	to determine the intensity of the smoothing. the greater the number of iterations, the smoother the surface.
<b>4</b>	<i>Surface mesh</i>	to set criteria for adding extra smoothness to part surfaces, and to set the criteria for improvement of the quality of surface mesh elements, relatively flat areas of the surface being preferentially smoothed compared with more curved areas. Surface smoothing will always tend to reduce the volume of a part. It will also reduce the quality of surface mesh elements but this can usually be corrected during optimization.
<b>5</b>	<i>Adapting the internal mesh</i>	the mesh node and element numbers can be reduced by re-meshing the interior mesh of parts into larger voxel (brick) elements. This preserves mesh density at the surface of parts (usually the region of interest) whilst reducing mesh density in part volume. When adapted, a part's mesh will always have significantly fewer nodes; element numbers will be reduced most effectively when the part has both large volume and a low surface-to-volume ratio (fairly big size).

Table 4.4) In our case these parameters were set with the following values:

Mesh Type	Mesh Quality	Mesh Iterations	Surface mesh	Adapt. Int. mesh
mixed	0,3	2	Add. Smoothing, optimize quality, Aggressive, Allow off surface	4x4x4

After that the FE-model obtained in Scan FE was exported as LS-DYNA file (\*.key).

**Skull part design**

Once the mesh of the brain and liquid interface was carried out the internal skull cavity was simulated in HyperMesh (Altair HyperWorks 9.0 ©) by generating a layer of shell elements wrapping the external surface of the liquid brain/skull interface, because this part was not possible to obtain from the segmentation process. This was due to the lack of Micro-CT images.

## 4.8 Materials and Properties Assignment

### Materials and Properties

In the literature survey different material data and model were investigated by Baumgartner D. (2009) and Hultman J. (2010). For the final selection of material data and model, a rat specific data and corresponding model was selected. The material data that selected comes from Haojie et al (2006) and can be seen in Table 4.5. The material model selected to describe the brain were a linear viscoelastic model, where in LS-Dyna 971 the corresponding material model was called Linear\_viscoelastic\_brain.

Table 4.5) The viscoelastic materials used in the simulation, taken form Haojie et al (2006).

Viscoelastic Materials					
Part in the model	Short term [kPa]	Long term [kPa]	Decay constant [ms]	Bulk modulus [GPa]	Density [kg/m <sup>3</sup> ]
Brainstem	3.10	0.92	20	2.19	1040
Caudate putamen	1.72	0.51	20	2.19	1040
Cerebellum	1.72	0.51	20	2.19	1040
Colliculi	1.72	0.51	20	2.19	1040
Corpus callosum	1.20	0.36	20	2.19	1040
Neocortex	1.72	0.51	20	2.19	1040
Hippocampus	1.72	0.51	20	2.19	1040
Olfactory bulb	1.72	0.51	20	2.19	1040
Ventricles	1.00	0.30	20	2.19	1040

Table 4.6) The elastic materials used in the simulation are listed below. Skull properties are taken from Baumgartner et al. (2004). The brain/skull interface behavior is inferred from studies from Zhang et al. (2001) and Mao et al. (2006, 2008).

Elastic Materials				
Part in the model	Property	Density [kg/m <sup>3</sup> ]	Young modulus [MPa]	Poisson's ratio
Brain/Skull interface (CSF)	Liquid interface	1130	20	0.45
Skull bone	Skull	2000	15000	0.22

## Boundary condition

The prescribed motion is calculated from the rotational acceleration curve seen in Figure 4.11. That velocity corresponds to an angular acceleration peak of  $1.5 \text{ Mrad/s}^2$  that is applied during  $0.5 \text{ ms}$ . The velocity is applied to the rat's head in the sagittal plane at its center of mass.

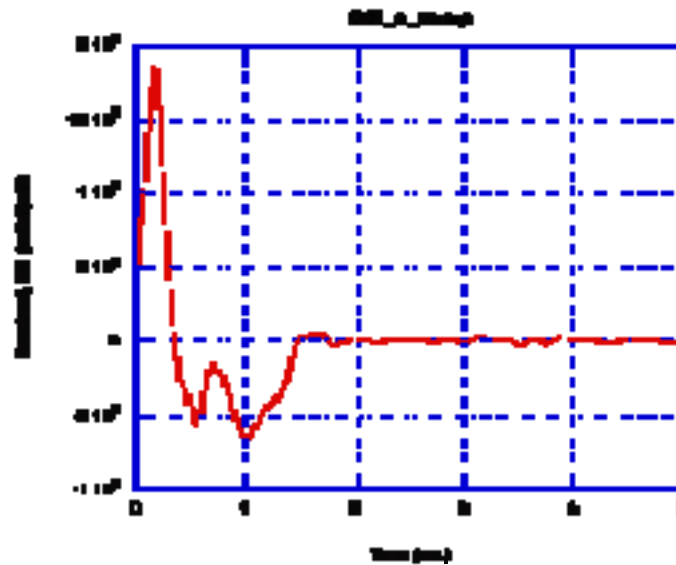


Figure 4.11. Rotational acceleration applied in the sagittal plane of the rat brain.



## 5. Results

In this chapter the results obtained through the method previously treated are following presented. The first part of this framework involves the results obtained by the initial MR images analyses in order to well understand the accuracy of these images. After that the results carry out by various segmentation processes are illustrated with different level of automation. Therefore, a way to check the final rat brain geometry is presented with the relative results. In the second part of this chapter the final result of the mesh generation process is presented, it is followed by a mesh quality evaluation. At last a quick evaluation of the FEM result is proposed.

### 5.1 MR Images analyses

First important step in this work is the MRI images acquisition, after that the original data can be imported into the software (SIP) for the segmentation process to obtain the 3D geometry final model.

From similar studies *Baumgartner D. et al (2009)* it is possible to deduce that to carry out this FE model T1, T2-weighted and CT-scan images are necessary. Unfortunately, in this work only T1-weighted MRI images were available with the information presented below.

*Tab. 5.1) The data consists of 128 slices with 128x128 pixels per slice, and each slice presents the following values listed in the table.*

<b>Modality</b>	MR	
<b>Patient's Name</b>	Rs_rat3D	
<b>Patient's sex</b>	F	
<b>Patient's Weight</b>	430 g	
<b>Slice Thickness</b>	0.26562 mm	
<b>X spacing pixels</b>	0.15625 mm	
<b>Y spacing pixels</b>	0.15728 mm	
<b>Repetition Time (TR)</b>	2500.08 ms	
<b>Echo Time (TE)</b>	78.975 ms	
<b>Flip Angle</b>	180	

These T1-weighted images present more imaging artifacts, such as low resolution, noise of the background, and poor contrast as it possible to see from the histogram in Figure 5.1. This leads to have several difficulties during the segmentation process and the geometry reconstruction.

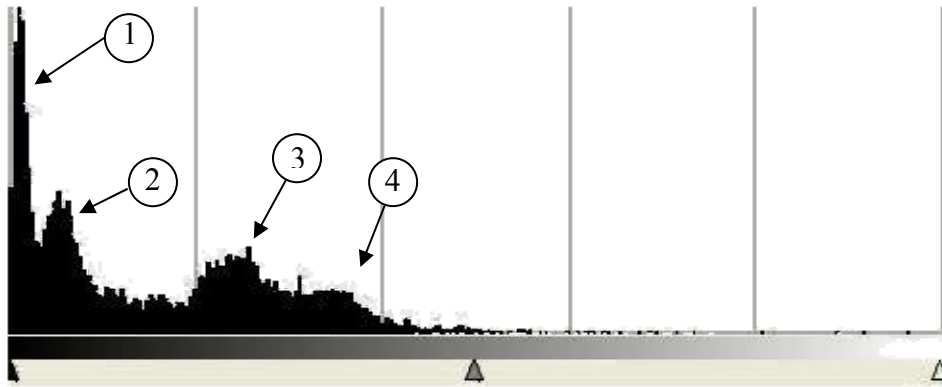


**Fig. 5.1:** Histogram of a MRI image from the original data

As showed in Figure 5.1, from the histogram of a MRI image of reference ( listed in Tab.5.1) it is possible to identify several peaks by dividing the intensity range in different windows of grayscale. Four peaks can be identified; the first on the left (1) shows the pixels belonging to the dark side of the background, thus it is not a region of interest for this work. The other three peaks are related to the brain region (3 and 4) and the liquid part (2); usually in T1-weighted images the CSF assumes lower intensity values than regions belonging to the brain in accordance with as said previously in paragraph 1.2.2 .

To improve the grayscale as well as the images contrast, several contrast enhancement operations were performed. The pictures below show an example of the result obtained from this operations and it can be seen that the image contrast was improved.

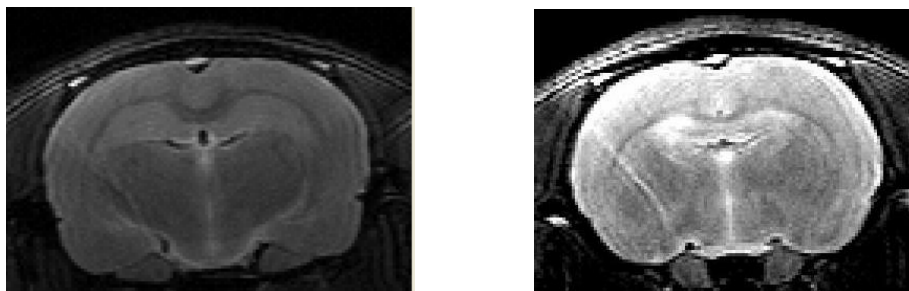


*Fig 5.3: The figure shows the original data (left) and the contrast enhancement effect (right)*

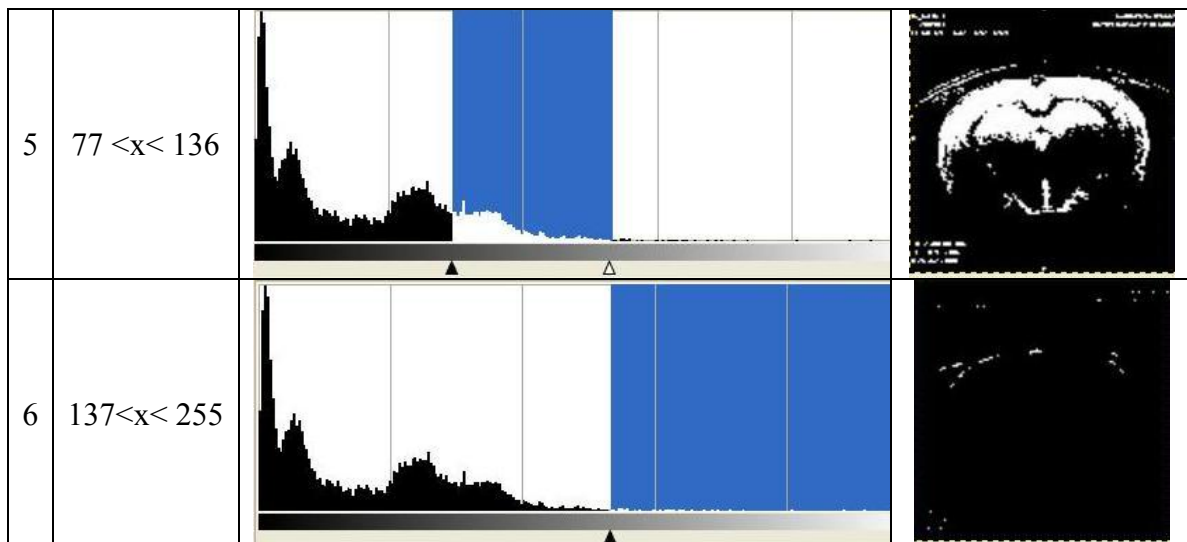
## 5.2 Geometry Results

### 5.2.1 Full-Automated Segmentation Results

In this step we evaluate the use of a Full-Automated approach to the segmentation process. This was carried out by using the *Threshold* function, by setting six different threshold values from 0 to 255, with “0” denoting darkness. This led to have six different windows (range) of grayscale into which the different brain region of interest should be identified.

*Table 5.2) The different windows of grayscale considered with the exact threshold value (x), the histogram and the final image result can be seen in the table. It is possible to notice how the white part of the histogram corresponds to the white part in the results.*

	Threshold range	Histogram	Result
1	$0 < x < 4$		
2	$5 < x < 25$		
3	$26 < x < 46$		
4	$47 < x < 76$		



Here the results listed in Tab. 5.2 are discussed. For each of the six different threshold values it was possible to make the following observations:

**1)  $0 < x < 4$**

In this range of gray scale should be included only totally dark pixels belonging to the background image, but, a lot of them were missed due to the presence of a lot of noise in the MRI images, as showed by the white part.

**2)  $5 < x < 25$**

This range includes the first peak of the histogram. This means that a brain region should be included into that grayscale range, which should be the CSF part because usually in T1-weighted MRI images this part is darker than the rest of the brain regions. As it is possible to see from the white zone on the picture, the result was not good enough because too much pixels not belonging to this area in the lower part of the image were included in the same grayscale range. This due to the noise and especially to the lack of T2-weighted MRI images, which leads to have a high pixels grayscale intensity belonging to the liquid parts, such as CSF.

**3)  $26 < x < 46$**

With this threshold value no peaks were included into this range, but it is possible to see how the upper part of the internal skull cavity and several pixels belonging to the Neocortex external boundary were included in the same grayscale.

**4)  $47 < x < 76$**

In this range of grayscale several brain parts were included. As showed in the result, it possible to identify the Thalamus, Hypothalamus, the upper part of the Corpus callosum and the lower part of the Neocortex. Unfortunately, all these parts were included in the same range of grayscale; therefore, it was not possible to identify one region from another separately.

**5)  $77 < x < 136$**

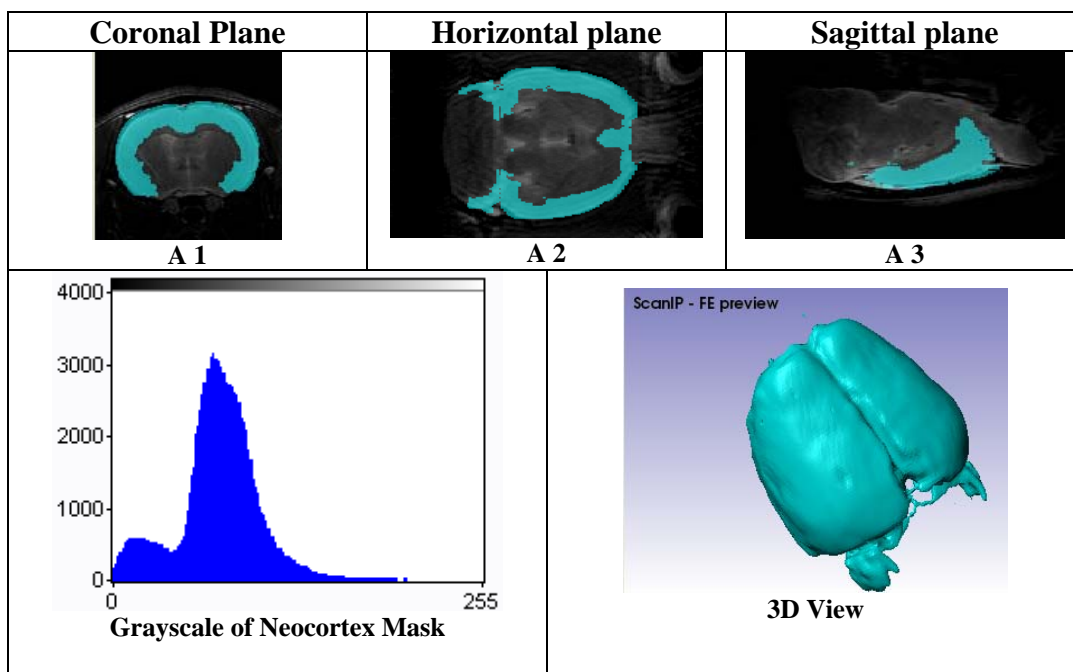
With this value it is possible to well identify the Hippocampus and the upper part of the Neocortex. As for the previous case both of these brain parts were included in the same grayscale range, therefore it was not possible to isolate them in different regions.

**6)  $137 < x < 255$**

In this range we could not get any result due to the overall low pixels intensity of the MRI images. As showed, all pixels were situated in the left side of the histogram with low intensity, thus half of the total range (0-255) was empty of pixels belonging to the brain.

As listed in the Table 5.2 a good segmentation was not obtained, due to the bad quality of the original MRI data. With these images we are able to carry out a good geometry by using the full-automated approach (by Thresholding) only if a less detailed model is required, without internal brain regions division. Maybe the thalamus region could be obtained but this region was not included into the list of regions in which we are interested in this study.

*Table 5.3) The results from the automated segmentation of the Neocortex are listed in table. In the first row of table 5.3 three different background cross sections with the segmented region are presented, in the second row it is possible to see the grayscale distribution from the histogram tool and the 3d view.*



The aim of this work is to obtain 10 different rat brain regions. A correct way to use the threshold function on these MRI images was trying to obtain the Neocortex geometry because it was the volume of interest (VOI) with higher dimension in the brain.

In one hand, it was quite easy defining the external boundary automatically by using a threshold value  $47 < x < 136$ , but in the other hand it was fairly hard to define the internal contours and interfaces with the other organs.

In Tab. 5.3 the results are listed and the following observations can be done:

- a) The results were fairly unsatisfactory to get the mesh; it was difficult to identify the boundary with the other neighboring organs in the lower part of the coronal view (A1) and the last part of the brain in horizontal view (A2). This is the largest region and therefore contains many pixels with different gray scales, especially in the lower part of the coronal view.
- b) From the histogram it's possible to see that a lot of pixels with a low intensity values are located at the left by generating a secondary little peak. The gray scale values should be reduced in order to eliminate this peak with low intensity and defining one intensity mean value with a standard deviation as low as possible.
- c) To tidy up the segmentation of this brain part a lot of manual fixing is required. It is possible to notice in Table 5.3 (Fig. A1, A2, A3) that the internal boundaries are very irregular and as a lot of pixels not belonging to this region were included in the last part of the brain (Fig. A2 and 3D view). This means a quite long time-consuming to refine this region.

At this point, not being able to realize the geometry of the FE model through the full-automated approach, we tried as much as possible to use a semi-automatic approach in order to minimize the operator intervention.

The semi-automatic approach consists of a combination with *region growing* algorithm tools (i.e. *Confidence connected region growing*) and several filters (Morphological and Gaussian).

## 5.2.2 Semi-Automated Segmentation

In this step the semi-automated approach is described and evaluated. This was carried out by using as much as possible the *Confidence connected region growing* function in the first step, and after a combination of manual fixing operation (i.e. paint and flood fill) and several filters were used to carry out the first geometry outline. The results of the following 9 brain regions are presented in the tables below. For each one of these regions (ROIs) the Histogram and the coronal view of the segmentation are presented.

Table 5.4.1, 5.4.2) *Ventricles, Hippocampus and Caudate putamen, Corpus Callosum, Colliculi and Cerebellum* results are listed in the tables below.

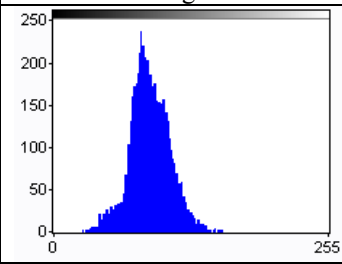
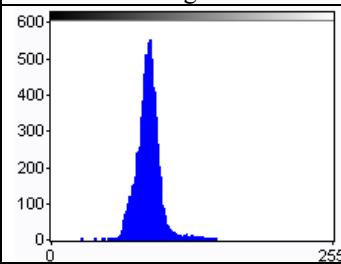
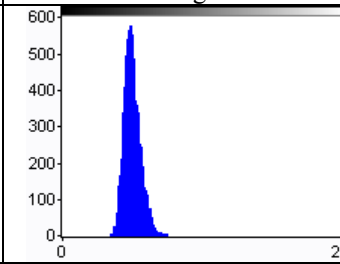
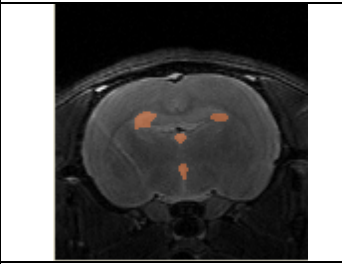
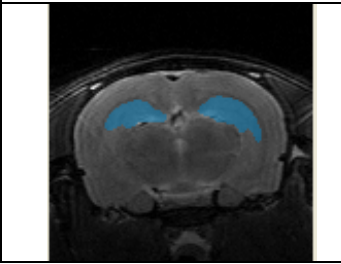
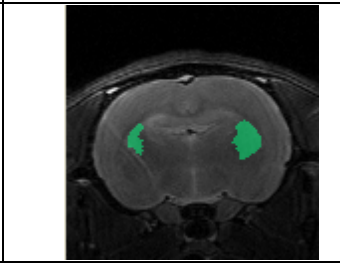
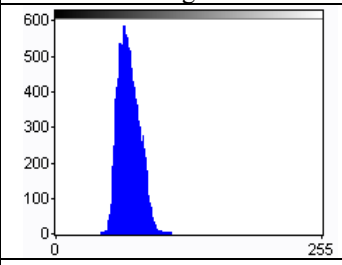
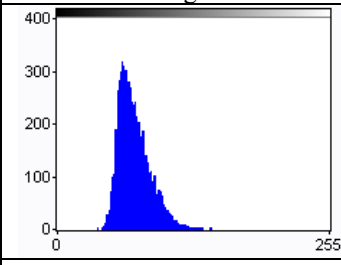
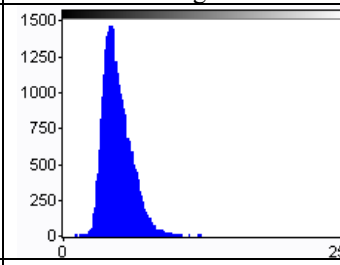
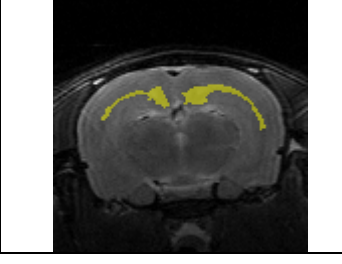
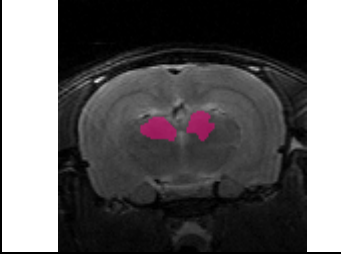
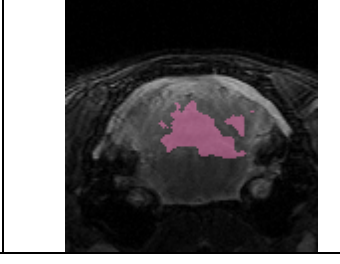
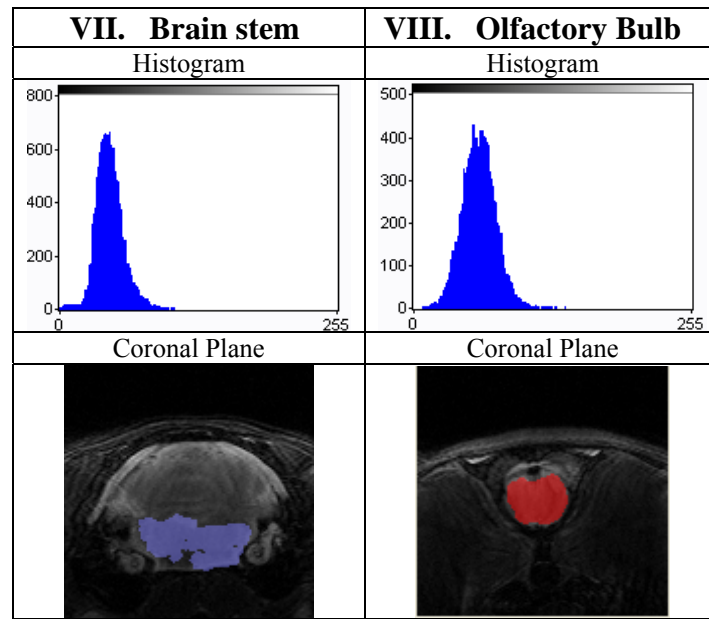
<b>I. Ventricles</b>	<b>II. Hippocampus</b>	<b>III. Caudate putamen</b>
Histogram	Histogram	Histogram
		
Coronal Plane	Coronal Plane	Coronal Plane
		
<b>IV. Corpus Callosum</b>	<b>V. Colliculi</b>	<b>VI. Cerebellum</b>
Histogram	Histogram	Histogram
		
Coronal Plane	Coronal Plane	Coronal Plane
		

Table 5.4.2) Brain Stem and Olfactory Bulbs results are listed in the tables below.



The discussion about the results obtained from each brain part (ROI) is following presented:

## I. Ventricles

The work on this ROI was very hard due to the poor image quality and especially to the lack of T2-weighted images. Once the final result was carried out we make the following observations:

- a) The result is considered not acceptable to generate the mesh due to the lack of information in the lateral part. It was quite difficult to identify the organ boundaries from the coronal and horizontal view, and part of hippocampus was wrongly included in the last part of the lateral ventricle. The worst result in the geometry was the symmetry; there is not symmetry on the lateral part.
- b) From the histogram it's possible to see that the grayscale range should be reduced by excluding the extreme values on the left and right with low *frequency of occurrence* and low pixels intensity not belonging to this ROI and by considering just that pixels with intensity values as close as possible to the mean intensity value of this ROI.

## II. Hippocampus

The initial segmentation of this ROI was carried out with a fairly acceptable result. It's possible to get the mesh, but it was difficult to define the boundaries between the hippocampus and lateral ventricle in both the coronal and horizontal views. As showed in the histogram the grayscale is well defined, with a quite high mean intensity value into the range considered (0-255), and extreme values with low *frequency of occurrence* due to the noise of the background was almost negligible, but a filtering operation was necessary to improve the results.

### **III. Caudate putamen**

The segmentation result of this region was carried out quite easily.

It was possible to get the mesh even if it was difficult to detect the boundaries with the hippocampus and lateral ventricle in both the coronal and horizontal views.

Grayscale was well defined, with a fairly high mean intensity value in the range considered, and low standard deviation because the extreme values were quite close to the mean values.

### **IV. Corpus Callosum**

The program was not able to get the mesh. It was difficult to detect the boundary with the other neighboring organs in the lower part of the coronal view and the last part of the brain in horizontal view. This was the thinner region, thus it could contain pixels with different gray scales belonging to other regions, especially in its lower part in the coronal view.

From the histogram it's possible to see how the standard deviation value was quite high and a lot of pixels of low-medium intensity were found at the left of the mean intensity value. The gray scale should be reduced in order to eliminate these pixels with low frequency of occurrence value in the range. This was achieved by only considering those grayscale intensity values closest to the mean value.

To tidy up the segmentation of this ROI many manual fixing is required.

### **V. Colliculi**

The result obtained from this region was acceptable enough to the mesh generation. The contours of this area were quite well defined for the segmentation and the gray scale was fairly well defined, with a few pixels of low frequency of occurrence on the right of the mean intensity value.

### **VI. Cerebellum**

The result was good enough to get a mesh; the contours are fairly well defined, except in the last part of the brain and along the part bordering the brain stem.

The grayscale is quite defined, although with a slight excess of pixels with low frequency of occurrence value in the right side of the range. The mean intensity value is quite low because in all the pictures the image contrasts the last part of the brain was very low.

### **VII. Brain stem**

This is the region with the worst result, it was possible to detect only the initial part of the brain stem, but we were not be able to define the rest of this region in the horizontal and sagittal view. Due to the fact that in this area the contrast is too low and the image is too dark, so you can not define the boundaries with the neighboring organs.

From the histogram it possible to notice that the gray scale intensity is much lower than other neighboring organs (i.e. cerebellum), and that many pixels with low intensity are present into the range.

To carry out the geometry from this region almost totally manual fixing was required, in order to tidy up the segmentation.

### VIII. Olfactory Bulb

The results obtained from this region could be acceptable to get the mesh; the boundaries of this area are quite well defined, except the initial part and the upper one of this organ due to low contrast and low image definition.

The gray scale was fairly defined, but the frequency of occurrence of pixels with the mean intensity value was not high enough and the standard deviation value was quite high because many pixels belonging to the surrounding brain regions were included on the right and left of the mean value.

To give the complete geometry to this part, some manual fixing was required in order to reconstruct the front and the upper part of this organ.

As listed in Table 5.5 a summary of the initial segmentation results is presented and the final observations are referred to the discussion of the final geometry.

*Tab 5.5) The summary of the segmentation results obtained by the semi-automated segmentation can be seen in the table.*

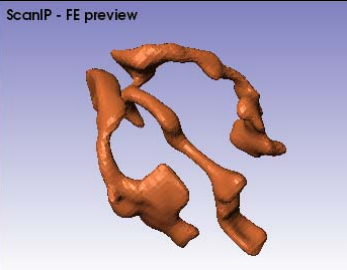
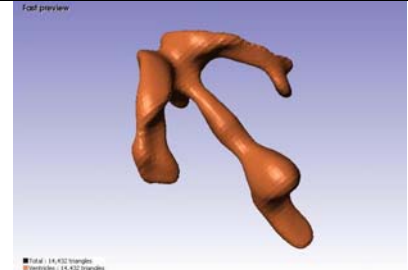
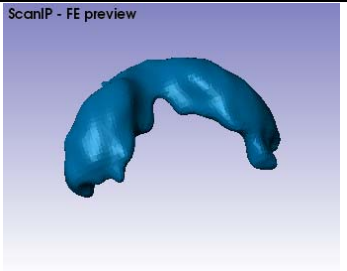
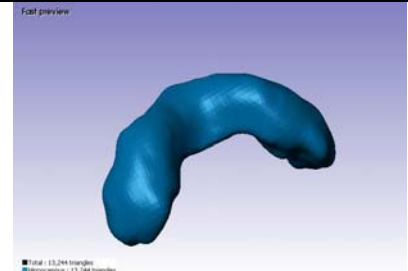
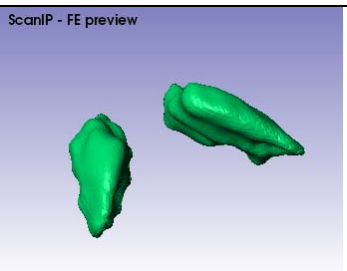
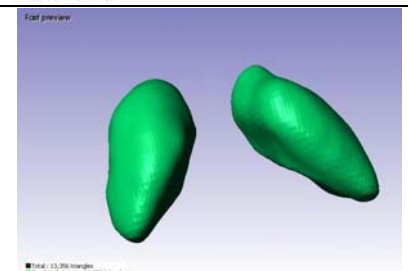
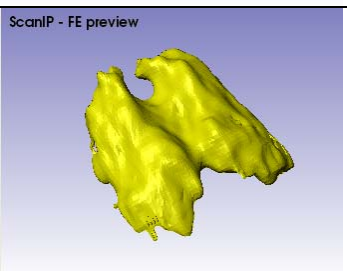
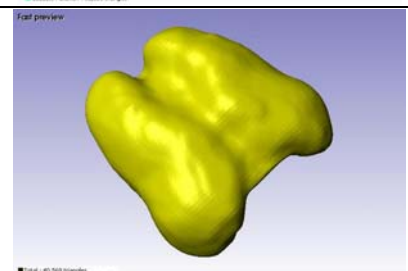
<b>n</b>	<b>Organ</b>	<b>Able to Mesh</b>	<b>Manual fixing</b>	<b>Area</b>
<b>1</b>	Ventricles	N	Partial	Last lateral part
<b>2</b>	Hippocampus	Y	-	
<b>3</b>	Caudate Putamen	Y	-	
<b>4</b>	Corpus Callosum	N	Partial	All/ Improve by hand
<b>5</b>	Neocortex	N	Partial	Lower and last part
<b>6</b>	Colliculi	Y	-	
<b>7</b>	Cerebellum	Y	Partial	Last part
<b>8</b>	Brain Stem	N	Total	All/ Draw by hand
<b>9</b>	Olfactory Bulb	Y	Partial	Upper and front part
<b>10</b>	Brain/Skull interface (CSF)	N	Total	All/ Draw by hand

### 5.2.3 Final Geometry Results

In this paragraph the results obtained by the refinement process are presented and discussed. This was achieved by starting from the initial segmentation results. The best solution to carry out a good segmentation involves having a marked difference in mean grayscale intensity between neighboring regions and the standard deviation values as low as possible, thus having a good images contrast.

The results of different brain parts obtained from the refinement process are presented below in several tables. With the *surface to volume ratio* we can have an idea about the size of the brain region considered, the lower is the ratio the larger is the size.

Tab 5.6.1) The geometry results before and after the final masks refinement are listed in the table by including some information about volume, surface and surface on volume ratio (s/v).

N	Initial geometry results	Final results	Vol. mm <sup>3</sup>	Surf. mm <sup>2</sup>	S/V ratio
1			77.3	287	3,69
2			86.9	231	2,73
3			113	246	2,16
4			239	764	3,17

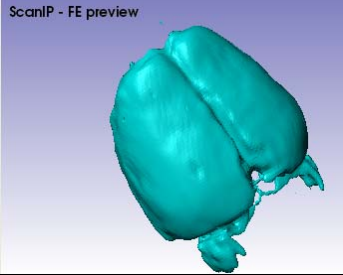
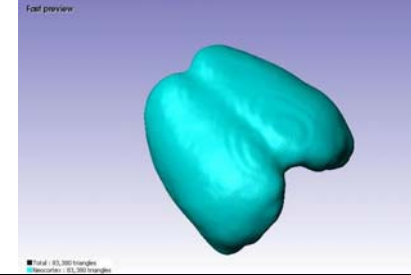
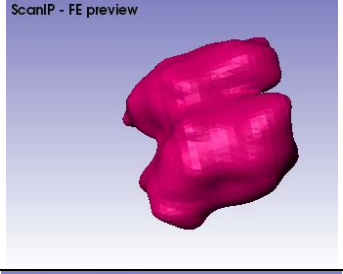
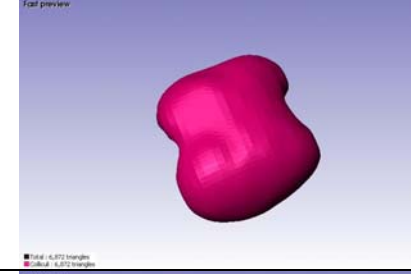
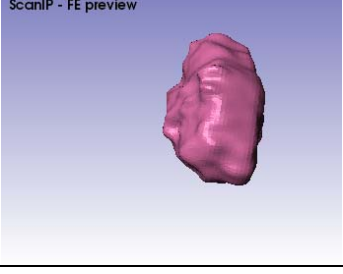
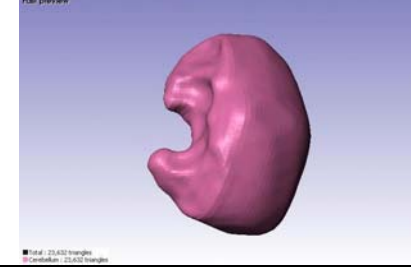
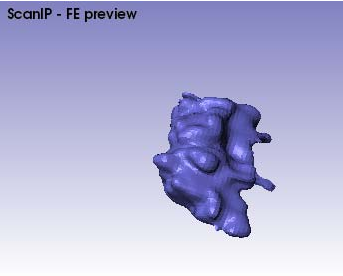
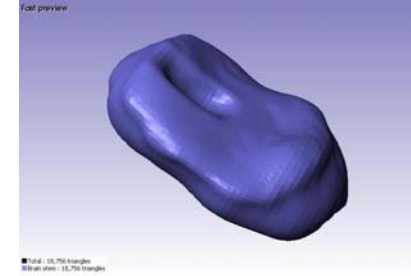
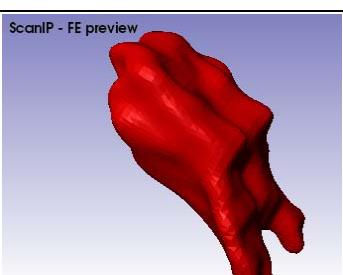
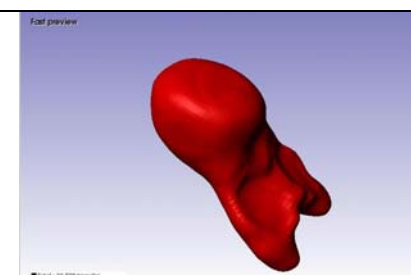
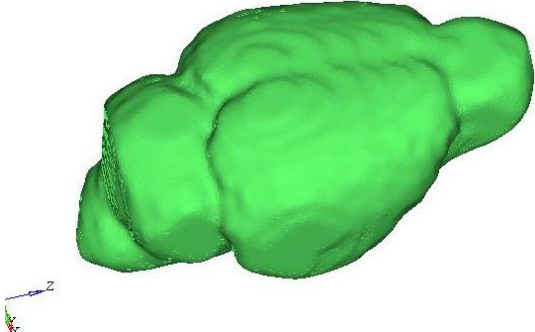
5	 <p>ScanIP - FE preview</p>	 <p>Fast preview</p> <p>Total: 83,380 triangles        Nonconvex: 63,260 triangles</p>	872	1490	1,74
6	 <p>ScanIP - FE preview</p>	 <p>Fast preview</p> <p>Total: 6,872 triangles        Nonconvex: 6,872 triangles</p>	46.4	122	2,58
7	 <p>ScanIP - FE preview</p>	 <p>Fast preview</p> <p>Total: 23,632 triangles        Nonconvex: 23,632 triangles</p>	342	404	1,21
8	 <p>ScanIP - FE preview</p>	 <p>Fast preview</p> <p>Total: 18,794 triangles        Nonconvex: 18,794 triangles</p>	263	338	1,31
9	 <p>ScanIP - FE preview</p>	 <p>Fast preview</p> <p>Total: 22,508 triangles        Nonconvex: 22,508 triangles</p>	272	393	1,45

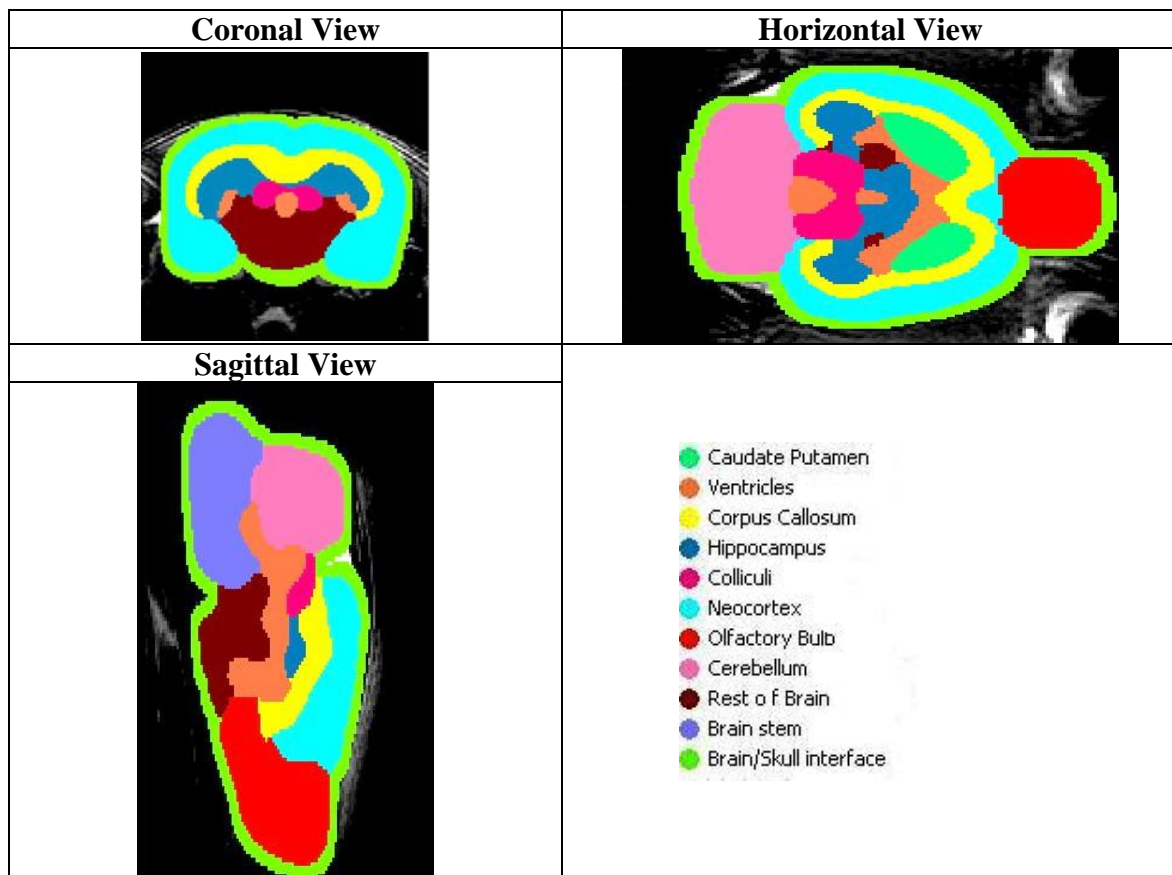
Table 5.6.2) The segmentation result of the CSF region can be seen in the table.

	<b>Brain / Skull Liquid interface (CSF)</b>	<b>Vol. mm<sup>3</sup></b>	<b>Surf. mm<sup>2</sup></b>	<b>S/V ratio</b>
10		846	3580	4,23

Tab 5.7) Several statistical data about the geometry and grayscale intensity, such as, voxels number, volume, mean intensity and standard deviation grayscale values are listed in the table.

<b>N</b>	<b>Mask</b>	<b>Voxels (x 1000)</b>	<b>Volume mm<sup>3</sup></b>	<b>Volume %</b>	<b>Mean Gray scale</b>	<b>Standard Deviation Grayscale</b>
1	Ventricles	11,835	77.3	2.98	75.5	15.3
2	Hippocampus	13,306	86.9	3.35	87.1	14.3
3	Caudate Putamen	17,245	113	4.36	62.6	8.08
4	Corpus Callosum	36,545	239	9.22	78.4	13.6
5	Neocortex	133,517	872	33.63	67.7	30.8
6	Colliculi	7,108	46.4	4.70	72.7	15.8
7	Cerebellum	52,453	342	13.19	50.7	21.0
8	Brain Stem	40,349	263	10.14	31.9	13.3
9	Olfactory Bulbs	41,645	272	10.49	50.6	23.6
10	Brain/Skull interface	129,544	846	24.60	30.6	29.2
11	Rest of brain	31,573	206	7.94	63.0	12.3
	<b>TOTAL</b>	<b>515,120</b>	<b>3360</b>	100	<b>53.5</b>	<b>30.4</b>

Tab 5.8) The final segmentation result of different brain regions can be seen in the coronal, sagittal and horizontal plane in order to identify the different bordering regions of each ROI.



To analyze and evaluate the results we focused on several parameters such as volume, the percentage of volume that each region occupies in relation to the whole brain volume and especially the difference in grayscale intensity between neighboring regions. By these parameters it was possible to compare the different mean and standard deviation grayscale values of each region.

The values of mean and standard deviation grayscale listed in Table 5.7 are showed in the graph below (Fig. 5.4) in order to better recognize of the difference in means gray scale between different ROIs.

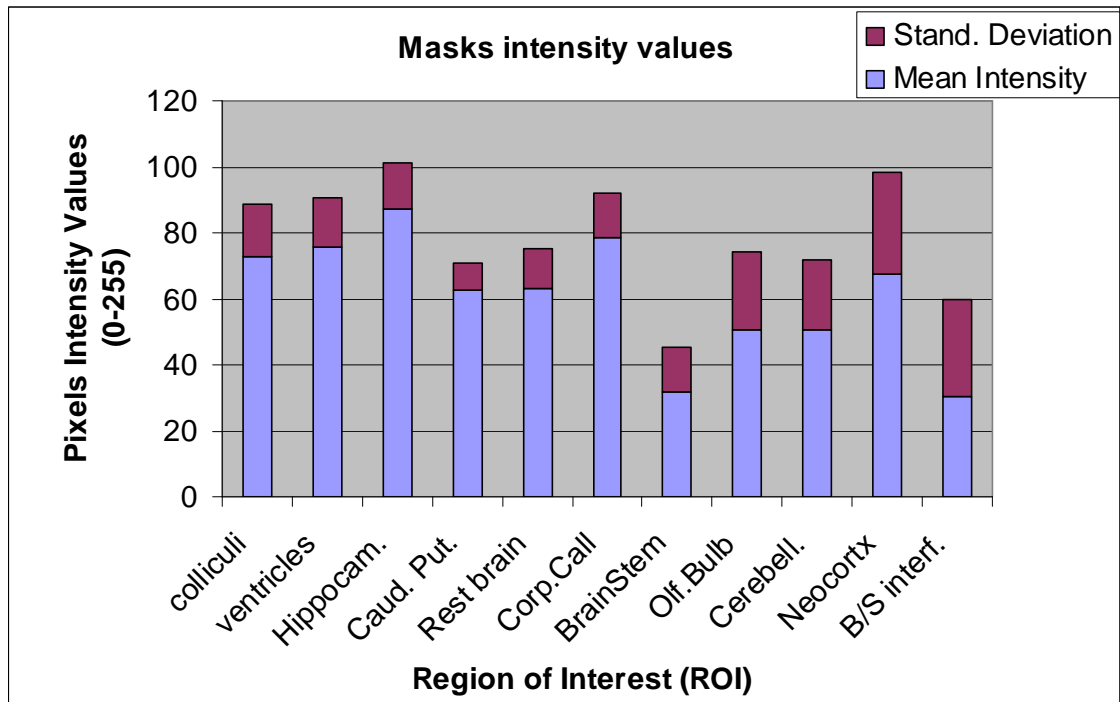


Figure 5.4: Grayscale Intensity and Standard deviation values of different ROIs

Tab 5.10) The segmentation results with high standard deviation values are showed in the table to notice several result limitations.

Brain stem	Olfactory bulb	Cerebellum	Neocortex
Grayscale Histogram	Grayscale Histogram	Grayscale Histogram	Grayscale Histogram
Coronal Plane	Coronal Plane	Coronal Plane	Coronal Plane

Table 5.10: Limitations of segmentation process

The discussion on the final geometry result, part by part, of the 10 brain regions and CSF part is presented below.

### *I. Ventricles*

The last part of the lateral ventricle has been improved by eliminating the part not belonging to this ROI as showed in Tab 5.6.1 part 1; the geometry has been improved by working with morphological and smoothing filters, but it was not possible to improve symmetry due to the low quality of the image.

This 3D geometry part has a total surface of  $278 \text{ mm}^2$  and a volume of  $77.3 \text{ mm}^3$  (0.0773 ml), this means 2.98% of the total volume ( $3360 \text{ mm}^3$ ).

From Table 5.8 it is possible to see the neighboring region connected with the ventricle region; all regions are connected with it, this means that a big difference of intensity between this region and the rest of the brain is required in order to obtain good result.

From the data in Tab 5.7 and 5.9 it possible to see how the pixels intensity value (Mean grayscale) of this region is too low compared to the rest of regions and its value is too much closer to the Corpus Callosum, Colliculi and Neocortex values due to the lack of T2-weighted images; this means that it was quite hard to define the boundary between the ventricle and these other brain parts by using fully-automated and semi-automated approach. Once the geometry has been completed, from Tab.5.7 it is possible to check the final Grayscale Standard deviation of this part, the value of 15.3 means that some extraneous pixels belonging to other regions were included, but not too much as at the beginning.

### *Hippocampus*

The initial segmentation of this ROI was carried out with quite good result as showed in Tab 5.6 part 2; to refine this mask some smoothing operation was performed in order to improve the surface quality and some extraneous pixels belonging to Corpus Callosum, Ventricles and Colliculi region were eliminated. As showed in Tab 5.8 and 5.9, these three regions are directly connected to Hippocampus and they have pixels intensity values fairly close to hippocampus mean grayscale value (87.1/255); this is the highest intensity value and for this reason it was one of the most easy to segment by using semi-automated method. The final volume of this region is  $86.9 \text{ mm}^3$  (0.0869 ml), 3.35% of the total volume with an external surface of  $231 \text{ mm}^2$ . From Tab.5.7 it possible to see the grayscale standard deviation close enough to the mean grayscale value, this means that the grayscale of this region is quite defined to use a semi-automated approach and to carry out an accurate geometry result.

### *II. Caudate Putamen*

This ROI is the one with best result. The initial segmentation was fairly good (Tab 5.6.1 part 3) because the grayscale of this region is well defined, as show in Tab 5.7 the mean grayscale value (62.6/255) is quite different from grayscale values of the neighboring regions, such as ventricles, corpus Callosum and olfactory bulbs, as showed in Tab 5.8 and 5.9. The standard deviation is the lowest of all (8.08) as showed in Tab 5.7, this means that this ROI presents the ideal requirement to obtain accurate geometry result by using a semi-automated segmentation process.

In Tab 5.6.1 and 5.7 it is possible to see the final result, it presents a surface of  $246 \text{ mm}^2$ , a volume of  $113 \text{ mm}^3$  (0.113 ml) and 4.36% of the total brain volume.

### III. *Corpus Callosum*

The results obtained with this ROI by the initial segmentation was not acceptable to get the mesh, a quite long refinement process has been done to improve the geometry, as showed in Tab 5.6.1 part 4. It was difficult to detect the boundary with the other neighboring organs in the lower and last part of the brain. In Tab 5.8 it is possible to see as there are a lot of different neighboring regions, such as: neocortex, caudate putamen, ventricles, hippocampus, colliculi and olfactory bulbs and from Tab 5.7 and 5.9 as the Corpus callosum mean grayscale value (78.4) is very close to that one of the other surrounding regions, such as ventricles (75.5) and colliculi (72.7). Thus was quite hard to define the boundary between these regions. The volume obtained after the mask refinement is of 263 mm<sup>3</sup> (0.263 ml) and 9.22% of the total brain volume with a surface of 764 mm<sup>2</sup> as listed in Tab 5.7.

### IV. *Neocortex*

The initial segmentation result of this ROI was not acceptable to get the mesh; it was difficult to detect the boundary with the other neighboring organs in the lower and last part of the brain. How showed in Tab5.8 there are a lot of neighboring regions, such as ventricles, corpus callosum, olfactory bulbs, cerebellum, colliculi and brain/skull interface (CSF).

In Tab 5.6.1 part 5, it is possible to notice the difference between before and after the refinement process. In the initial segmentation a lot of extraneous pixels belonging to neighboring regions are wrongly included in the last part of this ROI, as showed in the picture at the left. This is the largest region, therefore contains many pixels with different grayscale values especially in the lower part of the coronal view, due to the low quality of the images.

This can be notice from the grayscale standard deviation value of this region (Tab5.7), it is the highest value (30.8), and this means too much pixels with different grayscale are included in the same mask; another consideration could be done on the fairly low mean grayscale value (67.7/255), this means that pixels intensity was quite low and a lot of "dark" pixels belonging to the background were included, moreover, from Tab 5.9 it is possible to see how the Neocortex pixels intensity value is very close to that of ventricles and colliculi, thus was very hard to define the boundary between these regions. To carry out the final geometry a lot of smooth filtering operations were performed, but this led to a loss of detail in the external surface as showed in Tab 5.10, and that could be affect the result from the FEM analysis.

The final volume of this ROI is 872 mm<sup>3</sup> (0,872 ml), than 33.63% of the whole brain volume; with a total surface of 1490 mm<sup>2</sup>.

### V. *Colliculi*

The initial segmentation result of this ROI was carried out with quite good accuracy, and just some smoothing filter was used in order to drop the detail level of the geometry (Tab5.6.1 part6). The final volume is 46.4 mm<sup>3</sup> (0.046 ml), 4.7% of total brain volume and 122 mm<sup>2</sup> of surface. The main neighboring organs are: ventricles, hippocampus, corpus callosum, neocortex, cerebellum and rest of brain. From Tab 5.9 it possible to see how the ventricle and corpus callosum mean and standard deviation values are very similar to the values of this ROI (72.7 and 15.8 respectively), this involve a time-consuming to define the boundary of these regions.

## **VI. Cerebellum**

The initial segmentation result of this region needed to be improved especially in the last part of the brain, in which it was not possible to well define the boundaries of this region because the images were quite dark and with low contrast. This led to a quite long mask refinement process by using manual segmentation and several morphological filters; the final result can be seen in Tab 5.6.1 part 7, with the following values: volume  $342 \text{ mm}^3$  (0.342 ml) and 13.19% of the total brain volume, surface  $404 \text{ mm}^2$ . The neighboring regions are: ventricles, colliculi, brain stem, neocortex, rest of brain and brain/skull interface (Tab 5.8). From Tab 5.9 it is possible to see how the mean and standard deviation values of cerebellum and olfactory bulbs are very similar, but this was not really a problem because the two regions are not neighboring. On the other hand the neighboring regions have a different mean intensity value. This means that this body could be easily obtained by using semi-automatic methods, but this was not possible due to lack of image contrast in the latter part of the brain, moreover, it is possible to see from Tab 5.7 that the standard deviation value is quite high (21) because a lot of dark pixels belonging to the background were included in this mask during the manual segmentation refinement process.

## **VII. Brain Steam**

It was not possible to define this ROI by the initial segmentation, because in this brain part the image contrast and quality were very low, than the geometry was fully carried out by manual segmentation and quite long time was consumed to fix and tidy up this part. The final result is showed in Tab 5.6.1 part 8, with a volume of  $263 \text{ mm}^3$  (0.263 ml), 10.14% of the total brain volume and a surface of  $338 \text{ mm}^2$ . The neighboring regions are: ventricles, cerebellum, rest of brain and brain/skull interface (Tab 5.8), and from Tab 5.9 it possible to see how the grayscale mean value of this ROI is so close to that of the brain/skull interface, because several dark pixels belonging to the background were included.

## **VIII. Olfactory Bulbs**

The results obtained from the initial segmentation of this region could be good enough because the contours of this area are quite well defined, except the front and upper part of this organ, due to low contrast and low image definition. To carry out the complete geometry to this part, several manual fixing were required in order to reconstruct the upper and front part of this ROI, by using manual segmentation and several morphological and smoothing filters. The final result is showed in Tab 5.6.1 part 9 and it possible to see how the geometry volume was increased in the front and upper part with the following values:  $272 \text{ mm}^3$  (0.272 ml), 10.49% of the total brain volume and a surface of  $393 \text{ mm}^2$ . The neighboring regions with this ROI are: neocortex, corpus callosum, caudate putamen, ventricles, rest of brain and brain/skull interface, as showed in Tab 5.8. The grayscale of this ROI is quite well defined because its mean value is fairly different from that of the neighboring regions (Tab 5.7 and 5.9), but it possible to see how the standard deviation value is very high (23), this means that a lot of pixels with low intensity values were included in this region during the manual segmentation process to refine the geometry of this mask.

### ***IX. Brain/Skull Liquid Interface(CSF)***

This ROI was not possible to obtain by the initial segmentation process, because T2-weighted images were not provided for this work.

An alternative route to the initial segmentation was used, this ROI was obtained by creating a new mask joining the entire brain region mask in one through Boolean operations, the whole brain was dilated using morphological filters and then the whole brain was subtracted to obtain a thin mask wrapping the brain.

The final result can be seen in Tab 5.6.1 part10 and Tab 5.8, this new region has a volume of  $846 \text{ mm}^3$  (0.846 ml), 24.6% of the total model volume (brain and liquid interface), with a surface of  $3580 \text{ mm}^2$ . The mean grayscale intensity value of this region is the lowest because the pixels included belong to the background, thus with a low intensity, this can be notice from the high value of the standard deviation (Tab 5.7, 5.9) as well.

### ***X. Rest of the brain***

This is a “dummy” ROI; it has been created just to fill rest of the brain regions in which we are not interested.

In Tab 5.10 several examples with worse standard deviation are presented. It could be noticed as the two ROIs in which this problem is more evident are Olfactory bubs and Neocortex. In their histogram a secondary peak is present on the left of the mean intensity value; this means that a lot of dark pixels belonging to the background were included in the segmentation of these regions. This was due to the excessive use of morphological and smoothing filters in order to improve the external surface.

As outlined in both the coronal views of the same table, the refinement process led to several limitations in the geometry, such as the size of the olfactory bulbs and the loosing of detail in the Neocortex external surface.

### 5.3 Geometry accuracy evaluation

In this part of work we try to find a right way to validate the geometry results; the ideal solution should be to have the statistical data of the real geometry (in vivo) of the different brain regions, in which we focus on during this work. Unfortunately, during the literature survey this kind of data was not founded about rats, on the other hand a lot of data about mice was founded *Y. Ma et al. (2005)*.

The first step was finding a scaling law to use data from mice to rats in order to validate the geometry of the FE model. The difference between rat and mouse geometry was just in the size and volume of each organ, rat brain is 5 or 6 time bigger than mouse whole brain, as listed in Tab 5.11. Since it has not been possible to compare directly the volume values of each organ a different route has been used. We considered the percentage of volume occupied by each organ respect to the whole brain volume in which this organ belongs, then comparing this percentage of the same organ in both cases. The ideal result should be the same value for both cases in order to have a comparing ratio as close as possible to the unit value.

*Table 5.11) Statistical C57BL/6J mouse data taken by Y. Ma et al. (2005) was compared with the data obtained from the rat brain model and listed in the table.*

	RAT (Model)	MOUSE (Statistic)	Model/Stat. Ratio
Whole Brain (mm <sup>3</sup> )	2593,20	453,2	5,72
Colliculi	4,70%	3,16%	1,49
Ventricles	2,98%	0,33%	<b>9,01</b>
Hippocampus	3,35%	5,67%	0,59
Caudate Putamen	4,36%	5,87%	0,74
Rest of brain	7,94%	20,12%	0,39
Corpus Callosum	9,22%	3,27%	<b>2,82</b>
Brain Stem	10,14%	12,56%	0,81
Olfactory Bulbs	10,49%	5,05%	<b>2,08</b>
Cerebellum	13,19%	11,96%	1,10
Neocortex	33,63%	31,97%	1,05

The aim of this comparison was to evaluate in which brain region the error manifests itself most clearly. The Brain Stem values were not underlined because we are not interested to analyze this part. The exact error value was not calculated due to the lack of specific statistical data about rat brain geometry.

A second way to valuate these geometry results was performed by comparing the *surface to volume* ratio ( $s/v$ ) between the mouse statistical data and the rat brain model regions as listed in Tab 5.12.

Table 5.12) The surface on volume ratio of the different brain regions from statistical data (mouse) and rat model results (rat) was compared and listed in the table.

	mouse s/v	rat mod s/v
<b>Colliculi</b>	3,64	2,58
<b>Ventricles</b>	<b>11,00</b>	<b>3,69</b>
<b>Hippocampus</b>	3,05	2,73
<b>Caudate Putamen</b>	3,09	2,16
<b>Corpus Callosum</b>	<b>10,33</b>	<b>3,17</b>
<b>Brain Stem</b>	1,62	1,31
<b>Olfactory Bulbs</b>	2,13	1,45
<b>Cerebellum</b>	1,80	1,21
<b>Neocortex</b>	2,38	1,74

As listed in Tab 5.11 the main organs affected by a high geometric error are: ventricles and corpus callosum and olfactory bulbs; this information is very important to the final parametric study, because these three regions are seriously involved in the analysis of this FE model, than the final result could be affected by this geometric error.

We can see the distribution of the whole brain volume in its different component parts (or ROI), then comparing the rat geometry *model data* with the mouse *statistical data* by *Y. Ma et al. (2005)*.

With this operation it is possible to see as a good result (in term of volume) has been obtained with Colliculi, Caudate Putamen, Cerebellum, and Neocortex. On one hand we can see how the volume of Hippocampus, Brain steam and Rest of the brain is lower than statistical data values, and on the other hand the volume of Ventricles, Corpus Callosum and Olfactory bulbs is higher than statistical data values. That means during the segmentation refinement process the volume of Ventricles, Corpus Callosum and Olfactory bulbs was increased in order to improve the geometry, but this led to a decrease in volume of Hippocampus, Brain steam and Rest of the brain, even if we are not focus on the Rest of Brain part in this work.

From the graph showed below (Fig 5.5) it is possible to better recognize the error magnitude in the different brain regions (ROI) by using a ratio between geometry model (rat) and statistical data (mouse), and the unit value as reference value.

It is very clear as the ventricles geometry need a lot of improvement in order to decrease its volume without losing geometry information; that should be possible only by using T2-weighted images. The error value is quite high in corpus callosum and olfactory bulbs as well, because their volume was increased a lot by using filtering operations in order to get the correct geometry.

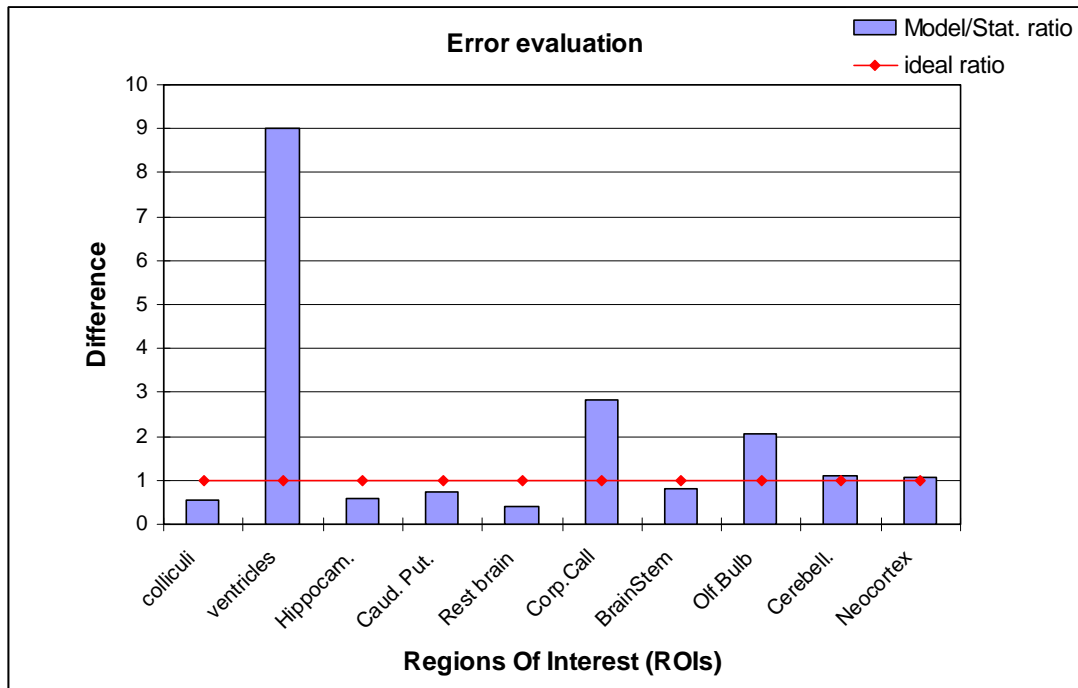


Fig. 5.5: Model on statistic data ratio of each ROI

A second way to compare the rat brain geometry results with the mouse statistical data was by using the surface on volume ratio (s/v). This parameter is useful because it considers the surface into which the brain region volume is wrapped; this leads to have an idea about the shape and size of the different brain parts.

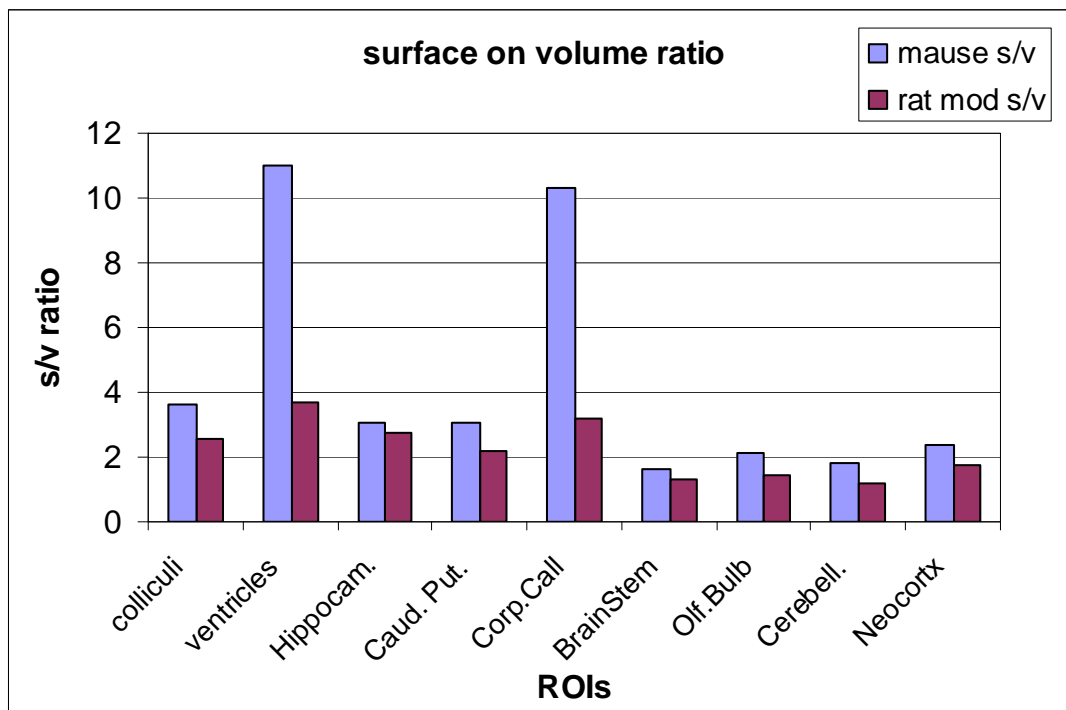


Fig 5.6: Comparison of Surface on Volume ratio between statistical data and result from the rat brain model.

We can see from Fig 5.6 as the  $S/V$  values of Ventricles and Corpus callosum belonging to the mouse statistical data are much higher respect to the rest of the mouse ROIs. This means that the volume of these two regions is very low and the surface is more irregular than the rest of brain regions.

Overall, the rat brain size is bigger than mouse (5 or 6 times as mentioned previously), than is quite obvious to have all the  $S/V$  rat brain model values down those of the mouse, but we can see as the Ventricles and Corpus callosum values of the rat brain model are too much far from the ones belonging to the mouse brain statistical data.

In the case of the statistic mouse data there is a lot difference in size between both ventricle and corpus callosum and the rest of the brain regions.

This means that the volume and surface of ventricles an corpus callosum belonging to the rat brain model need of improvements in order to decrease their volume and improve the surface detail.

In the literature review an experimental value of the CSF volume was found. By a statistical study of *Ramakrishna Nirogi et al (2008)* the volume of CSF collected from different rats varied from 100  $\mu\text{L}$  and 120  $\mu\text{L}$  (thus 0,10 and 0,12 ml). This value was compared with the one obtained from the rat FE model and it was noticed that the CSF volume belonging to the rat model was 10 times bigger than the reality.

## 5.4 Mesh Results

### 5.4.1 Elements density reduction results

The final result of this operation was achieved with a 0,3 mm value in X,Y,Z (*cubic resampling*). This process was called “*Resempling of data*” and led to a drop the total elements number of the whole brain and brain/skull interface (CSF) from 1,96 million to 660 thousand (mixed solution) as listed in Tab 5.13 and Tab 5.14.

Tab. 5.13) Geometry model Statistics values with original pixels spacing can be seen in the table.

ORIGINAL SPACING					
Mask	Voxels (x 1000)	Volume mm <sup>3</sup>	Surface mm <sup>2</sup>	hex/tetra elements	Surf./Vol. ratio
Colliculi	7,108	46.4	122	27,115	2,63
Ventricles	11,835	77.3	287	56,535	3,71
Hippocampus	13,306	86.9	231	51,727	2,66
Caudate Putamen	17,245	113	246	58,078	2,18
Rest of brain	31,573	206	363	92,718	1,76
Corpus Callosum	36,545	239	764	168,651	3,20
Brain Stem	40,349	263	338	97,737	1,29
Olfactory Bulbs	41,645	272	393	110,187	1,44
Cerebellum	52,453	342	404	124,915	1,18
Neocortex	133,517	872	1490	396,416	1,71
Brain/Skull interface	129,544	846	3580	0.78 M	4,23
<b>TOTAL</b>	<b>515,120</b>	<b>3360</b>	<b>8220</b>	<b>1.96 M</b>	

Tab .5.14) Geometry model Statistics values obtained by a cubic Resample Data operation with spacing of 0.3 mm in all directions are listed in the table.

REDUCTION OF ELEMENTS					
Mask	Voxels (x 1000)	Volume mm <sup>3</sup>	Surface mm <sup>2</sup>	hex/tetra elements	Surf./Vol. ratio
Colliculi	1,806	48.8	126	9,365	2,58
Ventricles	2,764	74.6	275	16,810	3,69
Hippocampus	3,409	92.0	251	18,248	2,73
Caudate Putamen	4,206	114	246	18,941	2,16
Rest of brain	7,704	208	354	29,823	1,70
Corpus Callosum	8,860	239	758	56,849	3,17
Brain Stem	9,886	267	349	32,564	1,31
Olfactory Bulbs	10,206	276	401	36,082	1,45
Cerebellum	12,821	346	419	39,900	1,21
Neocortex	32,202	869	1510	135,422	1,74
Brain/Skull interface	35,207	951	3580	261,992	3,76
<b>TOTAL</b>	<b>129,071</b>	<b>3480</b>	<b>8270</b>	<b>0,66 M</b>	

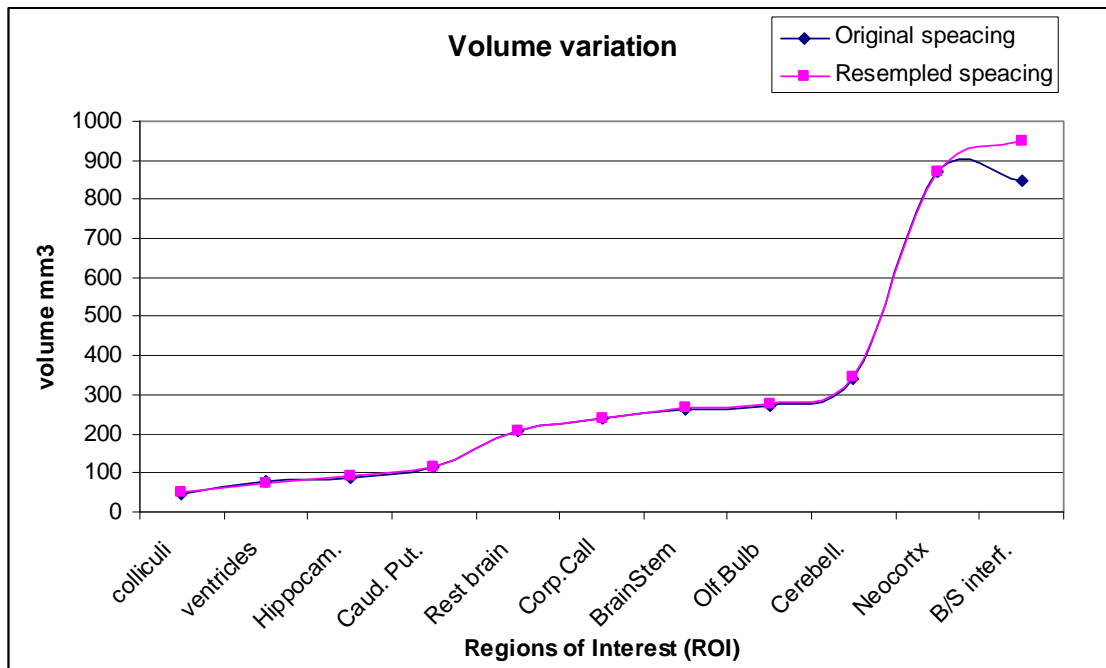


Figure 5.7: volume variation after data resempling operation

As showed in Fig 5.7, after the data resempling operation the volume value of almost all regions were not affected by changes except the brain / skull liquid interface (CSF), which increased its value from 846 to 951 mm<sup>3</sup> (0,95 ml).

This could also be noticed from the Surface/Volume ratio of the same organ in Tab 5.13 and 5.14, a decrease of this ratio indicates an increase in organ size.

### 5.4.2 Final Mesh Result

The first mesh result was carried out with Scan FE (simpleware®) by which all the brain regions and the CSF were meshed. As it is possible to see in Fig. 5.8, during the smoothing surface process tetrahedral elements were required along the interfaces and hexahedral elements were used where possible. An internal adaptation of 4x4x4 was used and this led to internal elements with bigger dimension in order to drop the element density.

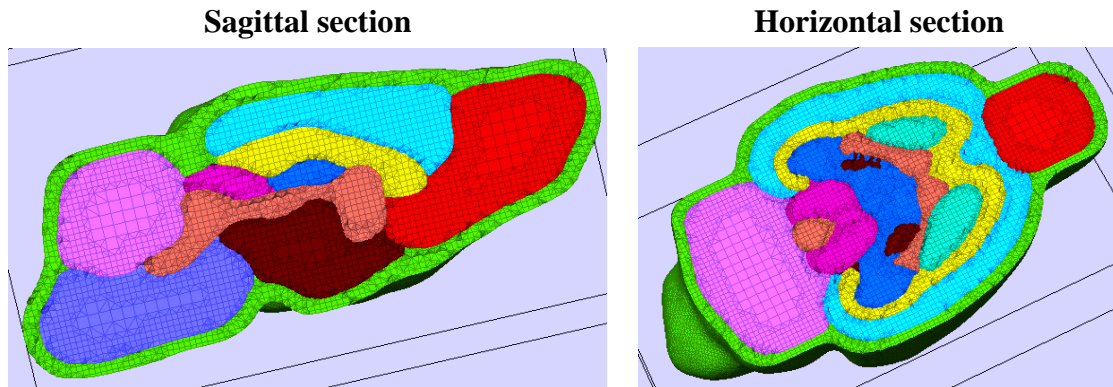
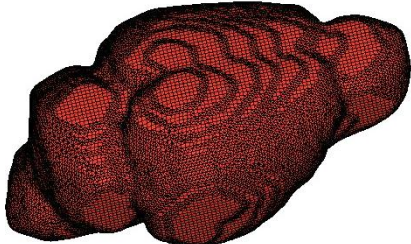


Figure 5.8: Mesh generation result from SFE

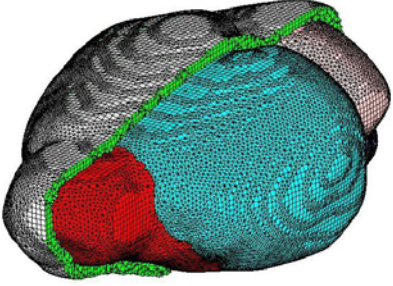
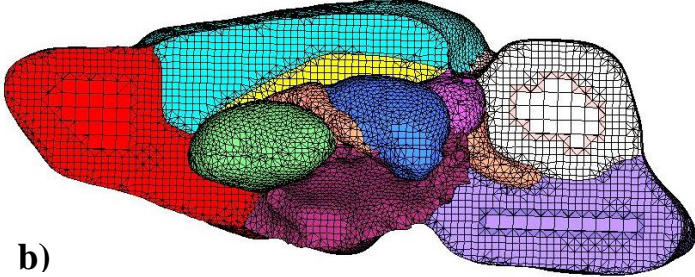
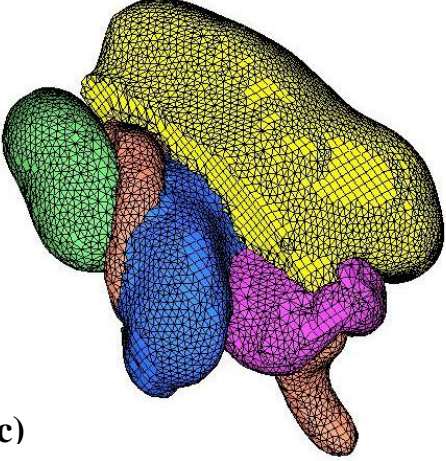
In the second step of the mesh generation the internal cavity of the skull bone was simulated by wrapping the CSF part, previously meshed in SFE (simpleware®), with shell elements. This result was achieved by importing the LS-DYNA file (\*.key) of this FE model, from Scan FE to HyperMesh (Altair HyperWorks 9.0 ©).

Table 5.15) The skull was simulated with one layer of shell mixed elements, as it can be seen in the table.

Skull part	Shell elements
	38,452

As listed in Table 5.15 this component was meshed with quads and triangular elements with a total number of 38,452 shell elements. This kind of 2D element was chose instead of solid elements in order to drop the total elements number of the rat brain FE model.

Table 5.16) The final mesh of the rat head FEM is showed in the table with different views: a) cross section of CSF and Skull internal cavity wrapping the whole brain, b) cross section in sagittal plane showing the cerebrum division in 7 different regions, c) implemented brain regions.

<b>Final Rat Brain FE Model</b>	
 <p>a)</p>	 <p>b)</p>
<b>Implemented Regions</b>	<b>List of Regions (ROI)</b>
 <p>c)</p>	<ul style="list-style-type: none"> <li><span style="color: green;">●</span> Caudate Putamen</li> <li><span style="color: orange;">●</span> Ventricles</li> <li><span style="color: yellow;">●</span> Corpus Callosum</li> <li><span style="color: blue;">●</span> Hippocampus</li> <li><span style="color: magenta;">●</span> Colliculi</li> <li><span style="color: cyan;">●</span> Neocortex</li> <li><span style="color: red;">●</span> Olfactory Bulb</li> <li><span style="color: pink;">●</span> Cerebellum</li> <li><span style="color: brown;">●</span> Rest of Brain</li> <li><span style="color: purple;">●</span> Brain stem</li> <li><span style="color: lightgreen;">●</span> Brain/Skull interface</li> </ul>

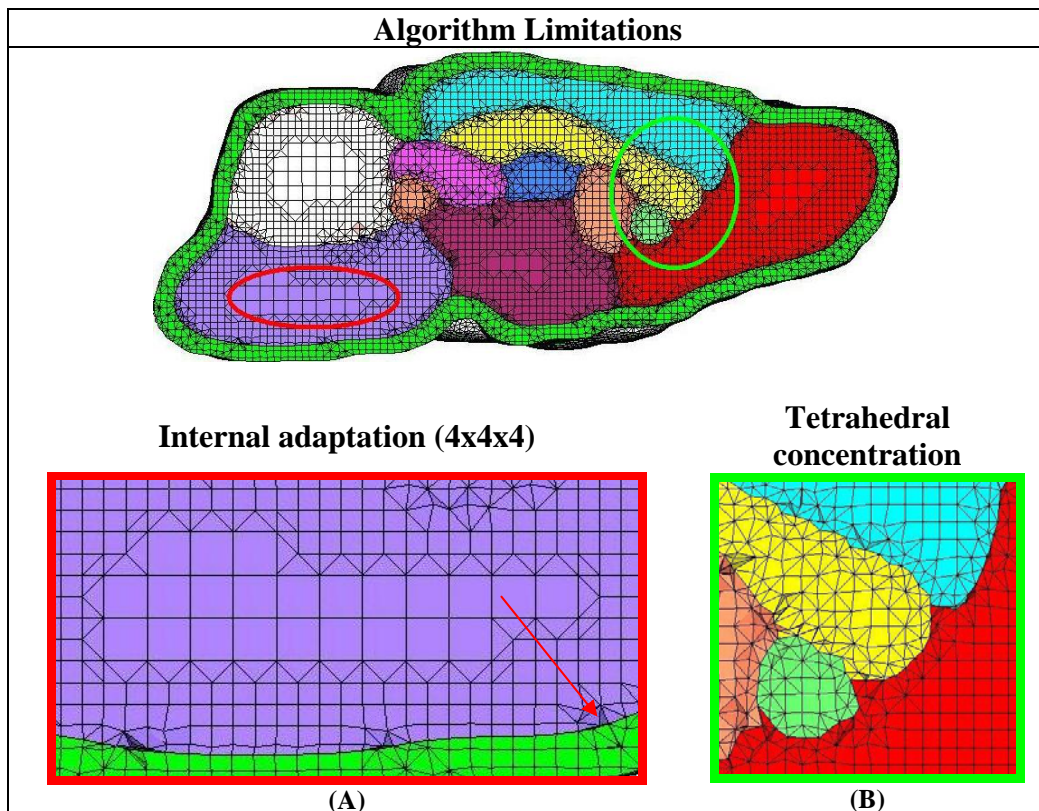
In the table 5.16, it can be notice as the cerebrum region detail was improved. This part was divided in the following 7 different regions: Neocortex, Corpus callosum, Caudate putamen, Vantricles, Hippocampus, Colliculi and Rest of the brain. This new rat head FEM consist in 38,452 shell mixed elements (triangular and quad) and in 676,225 solid mixed elements, which include 612,269 tetrahedral elements and 63,956 hexahedral elements. This led to a hexahedral on tetrahedral elements ratio of 10.4%.

## 5.5 Mesh Quality

### 5.5.1 SFE Algorithm Limitation

Once the final mesh was obtained, an analysis was performed to evaluate the performance of the meshing process and the algorithm (or meshing criteria) used in ScanFE (simpleware®). As listed in Table 5.17 the major limitation was the excessive presence of tetrahedral elements.

Table 5.17) The mesh limitations due to the SFE algorithm can be seen in the table.



The presence of tetrahedral elements is mainly due to two factors:

- I. *Internal adaptation setting*: this is an optional setting used during the mesh refinement operation to reduce the density of element by joining different hexahedral elements in one. The number of elements to join can be selected by the user and in our case was 4. The limitation consists in the presence of tetrahedral elements used to smooth the high difference in size between a big hexahedral (4x4x4) and a simple element as showed in Fig. A (Tab. 5.17).
- II. *Smoothing operations*: during this operation the external surface of each organ was smoothed by using tetrahedral elements where the surface presents a minimum curvature value as it is possible to see along the interface with the green part in Fig. A (Tab. 5.17).

## 5.5.2 Mesh Quality analysis

In this part a quality analysis of the final mesh was performed by using several metric criteria, such as warpage and jacobian. More criteria were used with the solid element, such as Tetra Collapse and Volume Skew in order to evaluate the tetrahedral elements quality by checking as many elements were included in the acceptable range of quality. These results were obtained by HyperMesh (Altair HyperWorks 9.0 ©) in which several reference threshold values were possible to set. In the tables bellow the results of Shell and Solid element analysis are presented.

*Table 5.18) The analysis results of the Shell elements belonging to the skull part are listed in the table.*

<b>2D Elements - Skull</b>				
<b>Metric criteria</b>	<b>Acceptable range</b>	<b>Failed elements (%)</b>	<b>Failed elements Number</b>	<b>Highest value out of the range</b>
Warpage	< 5	1	320	22.6
Aspect Ratio	< 5	0	0	-
Skew	< 60°	0	2	61.67
Chordal Deviation	< 0.1	0	0	0.00
Jacobian	> 0.7	0	179	0.58
Taper	< 0.5	0	0	0.46
Length min.[m]	> 1 e-04	0	13	0.82 e-04

*Table 5.19) The analysis results of the Solid elements belonging to the whole brain and CSF part are listed in the table by using several metric criteria.*

<b>3D Elements – Whole Brain and CSF</b>				
<b>Metric criteria</b>	<b>Acceptable range</b>	<b>Failed elements (%)</b>	<b>Failed elements Number</b>	<b>Highest value out of the range</b>
Warpage	< 5	5	34,192	26.39
Aspect Ratio	< 5	0	1,000	9.76
Skew	< 60°	2	12,112	77.40
<b>Tetra Collapse (1)</b>	<b>&gt; 0.5</b>	<b>33</b>	<b>202,662</b>	<b>0.14</b>
Jacobian (1)	> 0.7	1	4,755	0.30
<b>Vol. Skew (0)</b>	<b>&lt; 0.6</b>	<b>31</b>	<b>191,284</b>	<b>0.96</b>
Vol. AR	< 5	2	10,476	10.38
Length min.[m]	> 1 e-04	8	51,031	0.25 e-04

To better understand the results obtained from the Tetra Collapse and Volume skew criteria several measurements were performed as showed in the graph (Figure 5.9). This analysis was made in order to evaluate the tetrahedral elements quality.

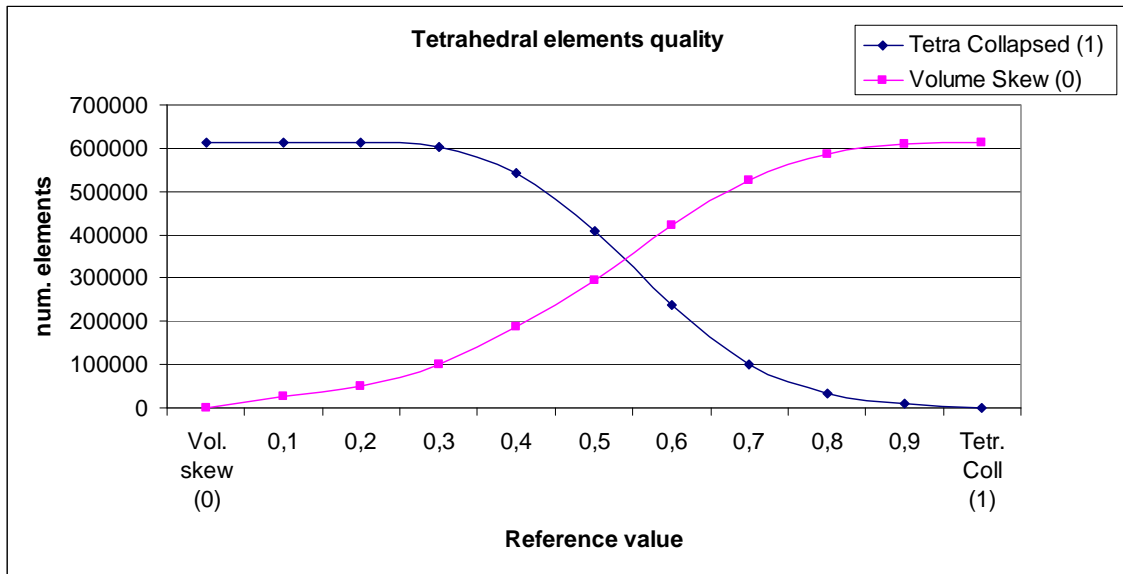


Figure 5.9: Tetra Collapsed and Volume Skew criteria results

It is possible to see as “0” and “1” are the reference values of Volume Skew and Tetra Collapse metrics respectively and notice as only less than 50% of elements have acceptable quality value (around 0.55) in both criteria.

## 5.6 FEM Reference Analysis

Once the final mesh was carried out the material properties and load condition were assigned in order to perform the reference analysis of this rat brain FE model. A detailed study on the simulation result of this FE model was performed by *Hultman J. (2010)*. The most interesting result was obtained with the brain plastic strain and share stress, as illustrate in figure 5.10. By these results it was possible to see the regions with high deformation and share stress to compare them with experimental data in terms of brain damaged areas.

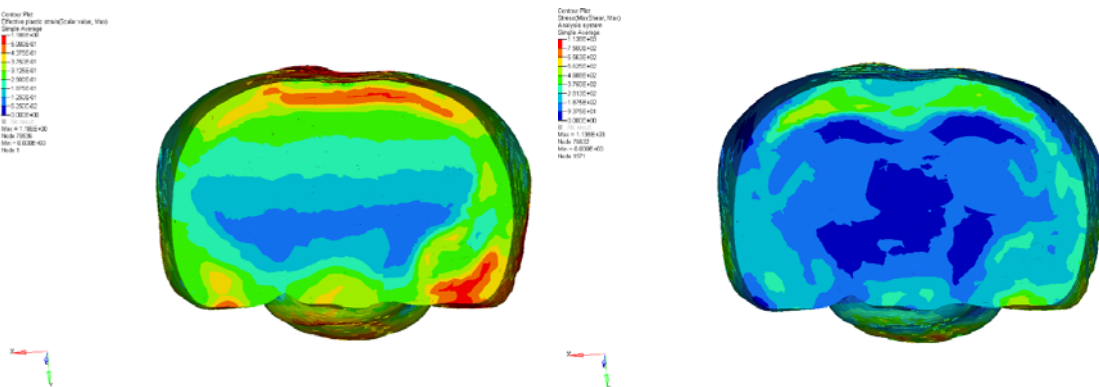


Figure 5.10: Brain plastic strain (left) and Share stress (right) 2.5 ms after the beginning of the impact.

The logarithmic strain can be seen in fig.5.10 (left), it varies from 0 – 50% with the highest value in the top of the brain and on the lower sides of the coronal plane. As showed in fig.5.10 the maximum shear stress in the section (right) was approximately 500 [Pa] and this value was found at the location of the injury. This means that there is a connection between injury and shear stress. Several observations were made about the brain pressure distribution. As showed in figure 5.11, a smoothed pressure distribution was not possible to obtain with this FE model.

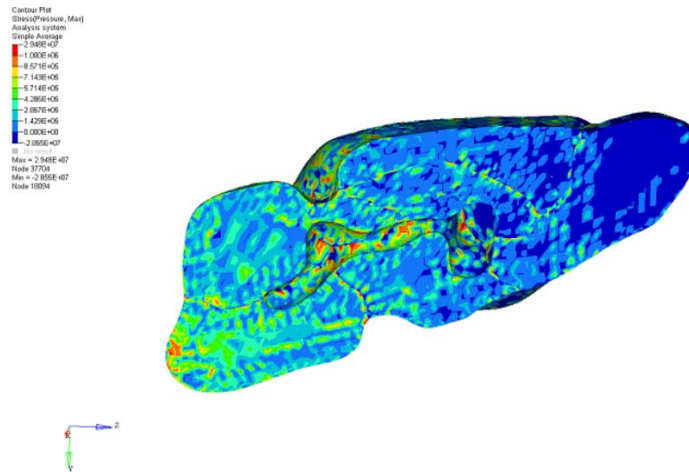


Figure 5.11: Brain pressure distribution 0.8 ms after the beginning of the impact.

Due to the high percentage of tetrahedral elements the pressure value increase locally until a maximum value of 2.8 MPa (red parts in fig. 5.11) where these elements are present. In the simulation it was seen the pressure wave and its movement inside the brain during the first 2.5 ms. To extract a rough value of pressure of this wave only one hexahedral element was selected in the central part of the olfactory bulb. The maximum pressure value loaded in this part of the brain was around 200 kPa.

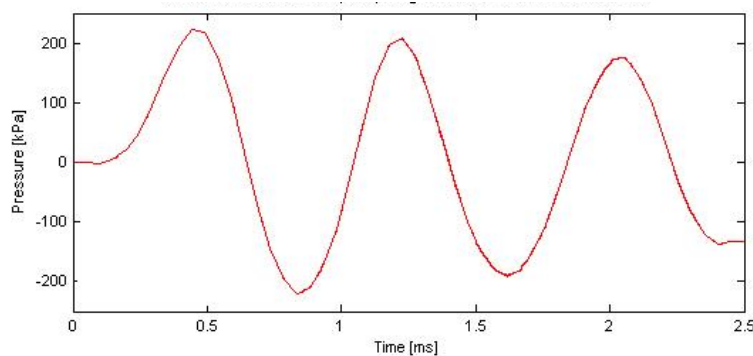


Figure 5.12: Pressure evolution in one hexahedral element inside the olfactory bulb.

As showed in figure 5.12 and 5.11, after 0.8 ms the pressure in the olfactory bulb assume a maximum negative value around 0.2 MPa and it corresponds to the darkest blue in the frame of simulation in figure 5.11. At the same time a maximum positive value was present in the opposite side of the brain, exactly in the last part of the brain stem region.



## 6. Discussion

### 6.1 Data Analysis

From the data listed in Tab 5.1 we can realize that the dimensions of the space involved in the scan process. This means 34 mm on Z axis ( $128 \times 0.26562$ ) and 20 mm on X and Y axis ( $128 \times 0.15625$ ), which lead to a total volume of  $13,6 \text{ cm}^3$ . An important aspect to be notice in these MRI images is the contrast mechanism by which they were obtained. These MRI were provided by Karolinska Institute (Stockholm) as T1-weighted images. By a literature survey *Prince J.L. et al (2005)* some reference values about the contrast mechanism were founded.

Unfortunately, the main parameters used in the scanning process of the MRI images in this work would suggest a contrast mechanism more close to a T2-weighted scan than T1. The data seem like something in the middle between T1 and T2 weighted images, because the value of TR and TE are too high to be a T1-weighted (usually between 400 and 550 ms).

*Table 6.1: The reference values of different contrast mechanism used in MRI acquisition obtained from literature survey (Medical Imaging, signals and systems by Jerry L. Prince) are compared with the value of MRI images used in this work and they can be seen in the table.*

	<b>T1 weighted</b>	<b>T2 weighted</b>	<b>PD weighted</b>	<b>MRI used</b>
<b>TR</b>	short (400-550) ms	long ( $>2500$ ms)	long	2500.08 ms
<b>TE</b>	short (10-30) ms	long (80-120 ms)	short	78.975 ms

Another important observation could be done on the quality of the original MRI data.

As the histogram in Fig 5.1 shows, it is quite hard to define the different part into the brain by using a fully-automated approach because the majority of pixels have a low intensity value with a fairly uniform grayscale; this also means low images contrast.

To improve the quality of the images a contrast enhancement operation was performed.

As shows in the picture below (Fig.6.1), the image quality with a scan resolution of  $100 \mu\text{m}$  (right) in all directions is greater than MR images used by us, which have a  $156.25 \times 157.28 \times 265.62 \mu\text{m}$  scan-resolution in X,Y,Z respectively. It was better than others studies (i.e.  $500 \mu\text{m}$  in X,Y,Z by *Baumgartner D. et al 2009*) but not enough to get the detail level required by this model. In similar studies a  $47 \mu\text{m}$  or less scan-resolutions value was used; therefore, more the pixel size value decreases, more their number increases, thus the image resolution.

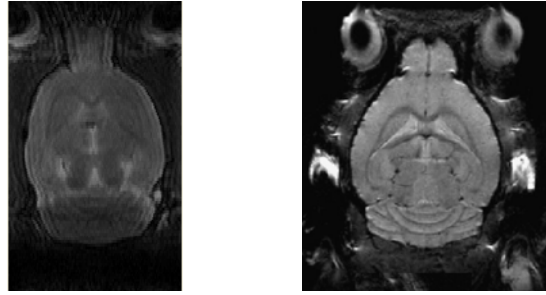


*Fig 6.1: Image from current data (left) and an Example of image with high resolution scan (100  $\mu\text{m}$  isotropic) from BrainWeb.*

The correct resolution value must be chosen based on the level of detail required by the model, so how many regions are needed to be segmented.

## 6.2 Final geometry evaluation

Overall, the MRI set used should have enough information to get the geometry of the whole brain only. The current resolution seems to pick out a lot of the features but the image contrast was too low to define all contour lines of each region in the last part of the brain. This led to have many difficulties to define several regions, such as Brain stem, CSF, Skull cavity and Olfactory bulb during the initial segmentation process.

From Tab 5.5 it can be notice as the brain regions with best results are: Hippocampus, Caudate Putamen and Colliculi; instead those with worse results are Corpus Callosum, brain stem and Brain/skull interface (CSF).The grayscale was not well defined, especially in several organs such as Neocortex and Corpus Callosum and automated function in the segmentation process were not possible to use.

A good segmentation result is required because the last step before the final mesh generation is the decreasing of number of elements. An acceptable segmentation result reduces the possibility of lacunas, such as missing pixels or holes in the mesh. Although at the same time this operation should not affect the geometry and continuity between surfaces of all organs.

At the end of the initial segmentation process it was possible to conclude that with the initial MRI images it was possible to optimize this model by using manual adjustments and several filtering operations through the segmentation refinement process, but without security about accuracy of results after the mesh generation.

The worst result of geometry was related to the Ventricles, Corpus Callosum, Olfactory bulbs and Brain stem, for different issues.

With the Ventricles part was not possible to obtain a good symmetry of the lateral part and its size was improved a lot in order to keep the geometry as smooth as possible.

The same was noticed with the Corpus Callosum and Olfactory bulbs, their final volume and size was increased in order to improve the external surface. This led to several limitations listed in Table 5.10.

It was possible to see from the histograms the overlapping of the grayscale values belonging to the different regions, thus why it was too hard identify the boundaries of

each brain region. The Brain Stem region was the hardest to carry out and its final part (spinal cord) was not possible to model because all images were too much dark in this region.

The geometry evaluation presented in chapter 5.2 led to the same conclusions about the Ventricles and the Corpus Callosum regions in accordance with as described previously. The major quantity of geometry error is present in these two ROIs. All these limitations could affect the accuracy of the FEM analysis results.

With the T1-weighted MRI images used in this work was not possible to get the CSF (brain/skull interface) part, thus an alternative route was used to model this part.

*The result leads to a CSF region geometry with a volume value around ten times bigger than the real case. This was due to the limitation of Scan IP because to correctly define a surface without discontinuity two rows of pixels at minimum are required. In our case each pixel have an edge of 0.3mm, thus it was not possible to model the CSF part with a thickness less of 0.6 mm.*

This observation is very important because this difference of values could affect a lot the dynamic of the model in the simulation and the FEM analysis results.

From other study on the automated segmentation performance valuation *Anjum A. Ali at all (2005)* it possible to notice which rat brain regions was more affected by error in the segmentation process. In that study the error value was calculated in term of difference (%) of overlapping, thus a high percentage value means a high error value in the geometry as show in Fig 6.2.

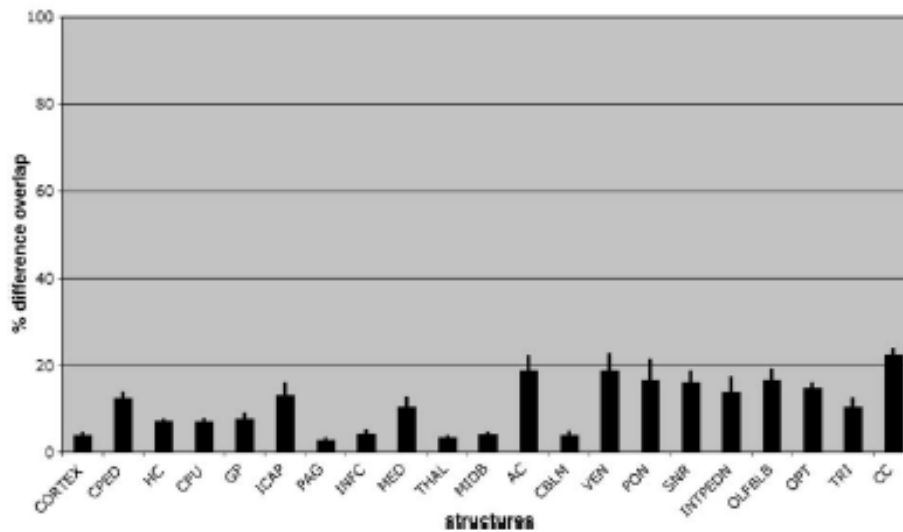


Figure 6.2: Example of geometry error results from automated segmentation (*Anjum A. Ali at all 2005*). CORTEX-Neocortex, HC-Hippocampus, CPU-Caudate Putamen, INFC-Inferior Colliculi, CBLM-Cerebellum, VEN- Ventricles, OLFBLB-Olfactory Bulbs, CC-Corpus Callosum

We can see how these results are conforming with the results obtained by our rat brain FE model and to the observations made during the geometry accuracy evaluation. In Fig 6.2 it possible to notice as the error value is high in the Corpus Callosum (CC), Olfactory Bulbs (OLFBLB) and Ventricles (VEN).

On other hand a low error value was found in Neocortex (CORTEX), Hippocampus (HP), Caudate Putamen (CP), Colliculi (INFC) and Cerebellum (CBLM).

Therefore, it is possible to conclude that the lack of good result in the segmentation, thus in the geometry, of Ventricles and Corpus Callosum results could also be related to the automated or semi-automated segmentation process and not just to the images quality. These two brain regions were the most difficult to obtain by automated approach because they are the ones with smaller dimension (highest s/v ratio) considered in this work. However, the extraction of their geometry was made even more difficult by the low MR image quality.

### 6.3 Mesh Results Evaluation

In the first step of the mesh generation density of the element was decreased by using Scan IP (simpleware®), then the geometry was imported in Scan FE (simpleware®) to the final mesh generation. The interior volumes of each part was adapted to increase the size of the elements in large volumes (4x4x4 was used), thus with a decrease in elements density. In Table 5.16 the final mesh result was presented.

In this new rat head FE model the number of brain region was increased by dividing the cerebrum part in 7 different regions in order to obtain a detailed model and improve the simulation results accuracy.

In the previous model (*Baumgartner D. et al 2009*) only four brain regions were included (Olfactory bulbs, Cerebrum, Brain Stem and Cerebellum) as well as the CSF and skull, which were simulated in HyperMesh (Altair HyperWorks 9.0 ©). Overall, it consisted in 17,972 hexahedral elements and 3,220 shell elements.

The new rat head model developed in this work includes 10 different brain regions apart from the CSF part and the skull internal cavity by including 676,225 solid and 38,452 shell mixed elements.

Due to the ScanFE meshing algorithm limitations listed in table 5.17, the final result consists in a high concentration of tetra-elements where there is a high presence of interfaces, thus where there is a high concentration of different brain regions (ROI). The tetra-elements concentration is even higher in those regions with a very irregular outer surface in which a lot of curves are generated.

From the technical support of ScanFE (simpleware®) were released the following ideal conditions to use this algorithm:

- a) Low Surface to Volume ratio
- b) Cubic pixels interspacing of 0.5 mm

This means working with big size geometry such as human body organs dimension in which a spacing of 0.5 or 1 mm is possible to use. Overall, the rat brain geometry developed in this work presents very small dimensions, thus with a quite high S/V ratio.

After starting from an original spacing of 0.15 x 0.15 x 0.25 mm it was improved to a maximum value of 0.3 mm in all directions by the *Resample data* operation, but a 0.5 mm value was not possible to use due to the low resolution of the original MRI images.

Probably the small dimension of the rat brain regions treated in this work leads to amplify these kind of limitations. From table 5.18 and 5.19 it possible to see how the dimension of the element edges was very small with a length min. in average around 0.1 mm and with a minimum value of 0.025 mm

An important limitation was the impossibility to define a different density of element separately for each different brain parts. This led to a high element density, which is strictly and only related to the voxel spacing previously chose in Scan IP (simpleware®).

The final result leads to a mesh with a hexahedral on tetrahedral ratio of 10.45% only and this could affect the final results accuracy in the reference analysis.

This ratio is strongly related to the surface on volume ratio ( $s/v$ ). This means that more the organ size is large, more the  $s/v$  ratio decreases, thus the hexahedral on tetrahedral ratio increases because the tetrahedral elements are used only to smooth the outer surface.

As showed in the table 5.18, the meshing of the skull is assumed to be regular in terms of edge, angle, warpage, aspect ratio, and others mesh quality metrics criteria.

All the shell elements have jacobian above 0.7. Overall, the number of elements with values out of the acceptable range is fairly negligible.

From the quality analysis of solid elements belonging to the whole brain and CSF part (Tab.5.19) was possible to see as the mesh was in the acceptable range of quality. Almost all the elements have a jacobian value above 0.5 (343 elements on 612,269 were failed only) and 99% of elements have a jacobian above 0.7.

In order to have more information on the tetrahedral elements geometry the Tetra Collapse and Volume Skew metrics criteria were used and they led to 33% and 31% of elements failed respectively. These metrics check the shape and geometry of the tetrahedral elements by comparing them with an ideal solution. This result notes as the quality of the tetrahedral elements was fairly low. This information is very important to the reference analysis because this rat brain FE model was composed by 89,55% of tetrahedral elements and this could seriously affect the simulation results accuracy calculated in LS-DYNA solver code.

## 6.4 FEM Results evaluation

In the end of this work it was quite surprising the correlation between injury and the simulation results obtained with strain and stress. Their level and location was roughly in the expected range except in several parts close the outer surface of Neocortex (fig. 6.3, right). As previously mentioned, the detail in the Neocortex outer surface was lost due to the heavy use of smoothing filters during the geometry generation.

A very important brain region treated in this work was the Corpus Callosum, but the size of this region obtained by the geometry generation was fairly greater than reality. This seems do not affect too much the simulation results because the interface between Neocortex and Corpus Callosum (fig.6.3, left) was not affected from this increasing of size. Maybe the brain regions located in the internal part of Corpus Callosum (i.e. Hippocampus and colliculi) could be affected by its increase in volume, but this can obviously affect the dynamic behavior of this FE model.

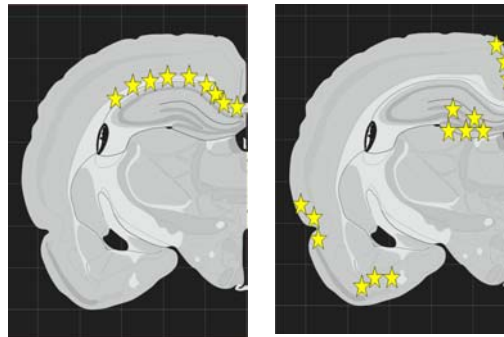


Figure 6.3: *The stars in the figure shows the axon injuries mapped by Davidsson J. et al (2009). This is the injury that the model was compared to (left). The stars are changes in the CoX2 mRNA activity (right).*

These maps could be used to compare the strain and stress along the Corpus Callosum/Neocortex interface and in the lower part of the Neocortex. The rest of stars on the Neocortex outer surface cannot be compared due to the loss of detail during the geometry generation.

On the other hand the increase in size of the other regions, such as olfactory bulb, ventricles and especially the CSF were heavily affecting the dynamic behavior of this FE rat head model during the simulation. The most important observation can be done on the Ventricles brain region and the CSF part. These two parts of the model were the ones with highest difference in geometry size with the reality. As previously seen in the geometry evaluation of this FE model, the Ventricles region was affected by error and asymmetry, and the CSF part results to be ten times bigger than reality. These geometric differences of these two parts can seriously affect the simulation results if they are treated as liquid, thus the entire geometry and behavior of the model will be affected by these error.

It was not a surprise the problems had with the pressure distribution. The high concentration of tetrahedral elements led to have a poor pressure response in the transition regions between different parts. Therefore it is hard to give any correlation between pressure and injuries on the rat brain.

## 7. Conclusions

The overall low quality of the MRI images used in this work led to have low accuracy in the geometry results. Especially, the low images contrast in the first and last part of the brain led to have a lot of difficulties to identify the boundary of the Olfactory Bulbs and the last part of the Brain stem (spine). A high-resolution scan with a more appropriate contrast mechanism would be necessary in order to make best use of the full-automated and semi-automated segmentation. The low image quality did not permit to model the rat brain geometry by using a full automated approach. With the T1-weighted MR images provided a semi-automated segmentation and manual refinement process were required.

Although, the excessive use of these filters to smooth and tidy up the geometry led to a loss of detail in the external surface of the Neocortex and an increase in volume of several brain regions, such as Olfactory bulbs, Ventricles.

The lack of T2-weighted MRI images led to have several limitations to identify the ventricles region, the CSF part and the boundaries of the surrounding regions. The worst result due to this lack was the CSF volume value, which was around ten times greater than the real value because it was not possible to get the correct geometry by the segmentation process.

The accuracy of the geometry results obtained by the semi-automated segmentation could be considered fairly acceptable by comparing the volume and size values between the rat brain model and mouse statistical data. It is obvious that the way used to make this comparison was not the most appropriate because several scaling laws between mouse and rat were used. By this geometry evaluation the brain regions with high difference in volume and size were the Ventricles, Corpus Callosum and Olfactory bulb in according with similar previous studies *Anjum A. Ali at all (2005)*.

The segmentation process used to extract the geometry has the following drawbacks:

- a) Less repeatability, because the semi-automated method has a less repeatability than full-automated method, thus even worst with the long refinement process used to tidy up the final geometry results. Because a lot users interaction was required in this last process.
- b) Time consuming, because a long period of time was spent to identify the different brain region before and to tidy up the geometry results after.

The detail level of this new rat brain FE model was improved respect to the previous one with a strong increase in total number of elements, but several limitations were founded during the mesh generation process. This problem was due to the Scan FE (simpleware®) algorithm limitations related to the overall low dimensions of the rat brain model. Moreover, in this software it was not possible to have a good control on the mesh generation with the setting tools available. This led to a high concentration of tetrahedral elements in the final mesh.

The simulation results obtained with stress and strain were fairly acceptable and a correlation with the injuries was possible to fund along the interface between Neocortex and Corpus Callosum, which was not possible with the previous model.

Unfortunately, the results obtained with pressure were not acceptable due to the wrong pressure distribution. The reason of this limitation was the excessive concentration of tetrahedral elements, as mentioned several times during this thesis.

Another interesting result obtained with this work was the correlation founded between initial data (MR Images) accuracy and simulation results. A very clear example is the CSF part; the lack of T2 images and especially the low contrast images and resolution led to have a wrong geometry by the segmentation process, thus the rat brain model dynamic behavior was affected during the simulation.

## 8. Future Work

As continuation of this work several point of study and improvements could be suggested:

- T1 and T2 weighted MR Images are required (CT eventually) with an acceptable contrast image and resolution (100  $\mu\text{m}$  isotropic or less) to get the model with the detail level required.
- Exact rat brain statistical data are needed to compare the geometry obtained by the segmentation process with the real ones, thus the exact geometric error value can be calculated.
- A way to improve the mesh quality should be found in order to reduce the elements density where it is not required and to convert as much as possible tetrahedral elements in hexahedral elements, especially in those regions studied during the simulation.
- A deeper study on the different material properties of the different brain regions would be very interesting as continuation of this work in order to evaluate if the model developed in this work is much more material dependent than mesh dependent.
- Define independent regions and create contact between them in order to study their mutual interaction
- A way to validate the simulation results should be found.

## References

A. Bade, A.A. Ali and G.A. Johnson (2007): *Morphometric analysis of the C57BL/6J mouse brain*. Duke University Medical Center, Durham, USA 2007

Anjum A. Ali, Anders M. Dale, Alexandra Badea and G. Allan Johnson (2005): *Automated segmentation of neuroanatomical structures in multispectral MR microscopy of the mouse brain*. University of California, San Diego, USA 2005.

Baumgartner D., Lamy M., Willinger R., Davidsson J., Choquet P., Goetz C., Constantinesco (2009): *Finite Element analysis of traumatic Brain Injuries mechanism in the rat*. University of Strasbourg and Chalmers University of Technology 2009.

D.W Mc Robbie, E.A. Moore, et al: *MRI from picture to Proton*.

Hultman J. (2010): *Using Finite Element simulations to reproduce rational induced brain injury experiments: Recommendations for the future*. Department of Injure Prevention, Chalmers University of Technology, Gothenburg, Sweden, 2010

John Ashburner and Karl J. Friston (2005): *Unified segmentation*. Department of Imaging Neuroscience, Functional Imaging Laboratory 12 Queen Square, London, UK 2005.

Johnson Ho, Hans von Holst, Svein Kleiven (2010): *Automatic generation and validation of patient-specific finite element head models suitable for crashworthiness analysis*. Division of Neuronic Engineering, School of Technology and Health, Royal Institute of Technology and Institute of Laboratory Medicine and Clinical Neuroscience, Karolinska Institutet, Stockholm, Sweden.

P. G. Young, T. B. H. Beresford – West, S.R.L. Coward, B. Notarberardino, B. Walker and A. Abdul-Aziz.(2008): *An efficient approach to converting three-dimensional image data into highly accurate computational models*. School of Engineering, Computing and Mathematics, University of Exeter, North Park Road, Exeter, UK 2008.

Paxinos G. and Watson C. (2007): *The Rat Brain in stereotaxic coordinate (6<sup>th</sup> edition)*. Published by Elsevier Inc. 2007

Prince J.L. - Links J.M. (2005): *Medical Imaging- Signals and Systems*. Prentice Hall.

Ramakrishna Nirogi, Vishwottam Kandikere, Koteswara Mudigonda, Gopinadh Bhyrapuneni, Nageswararao Muddana, Ramanatha Saralaya, Vijay Benade (2008): *A simple and rapid method to collect the cerebrospinal fluid of rats and its application for the assessment of drug penetration into the central nervous system*. Banjara Hills, Hyderabad, India 2008.

Simpleware Ltd. 2009 SCANIP and SCANFE software v. 3.2 reference guide. Exeter, UK: Innovation Centre.

Vance Unruh and David C. Anderson (1992): *Feature-Based Modeling for Automatic*

*Mesh Generation*. School of Mechanical Engineering, Purdue University, West Lafayette, IN, USA.

Y.Ma, P.R. Hof, S.C. Grant, S.J. Blackband, R. Bennet, L. Slatest, M.D. McGuigan and H. Benveniste (2005): *A three-dimensional digital Atlas database of the adult C57BL/6J Mouse brain by magnetic resonance microscopy*. New York, NY, USA 2005.

Zujun Hou (2006): *A Review on MR Image Intensity Inhomogeneity Correction*. Biomedical Imaging Lab., Singapore Bioimaging Consortium, Singapore.